

Supporting Information

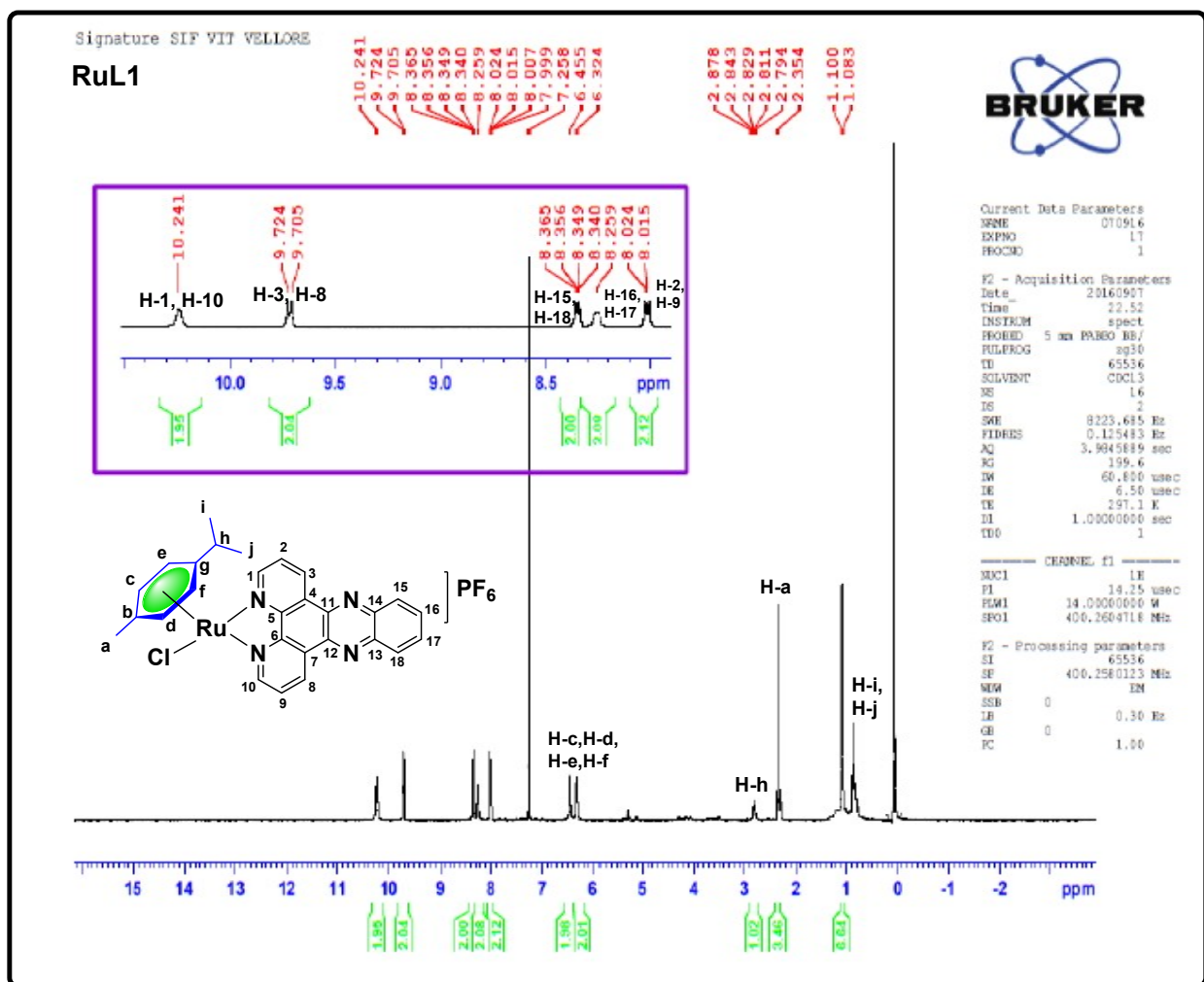
One pot three component synthesis of DNA targeting phototoxic Ru(II)-*p*-cymene dipyrido[3,2-*a*:2',3'-*c*]phenazine analogues

Binoy Kar, Priyankar Paira*

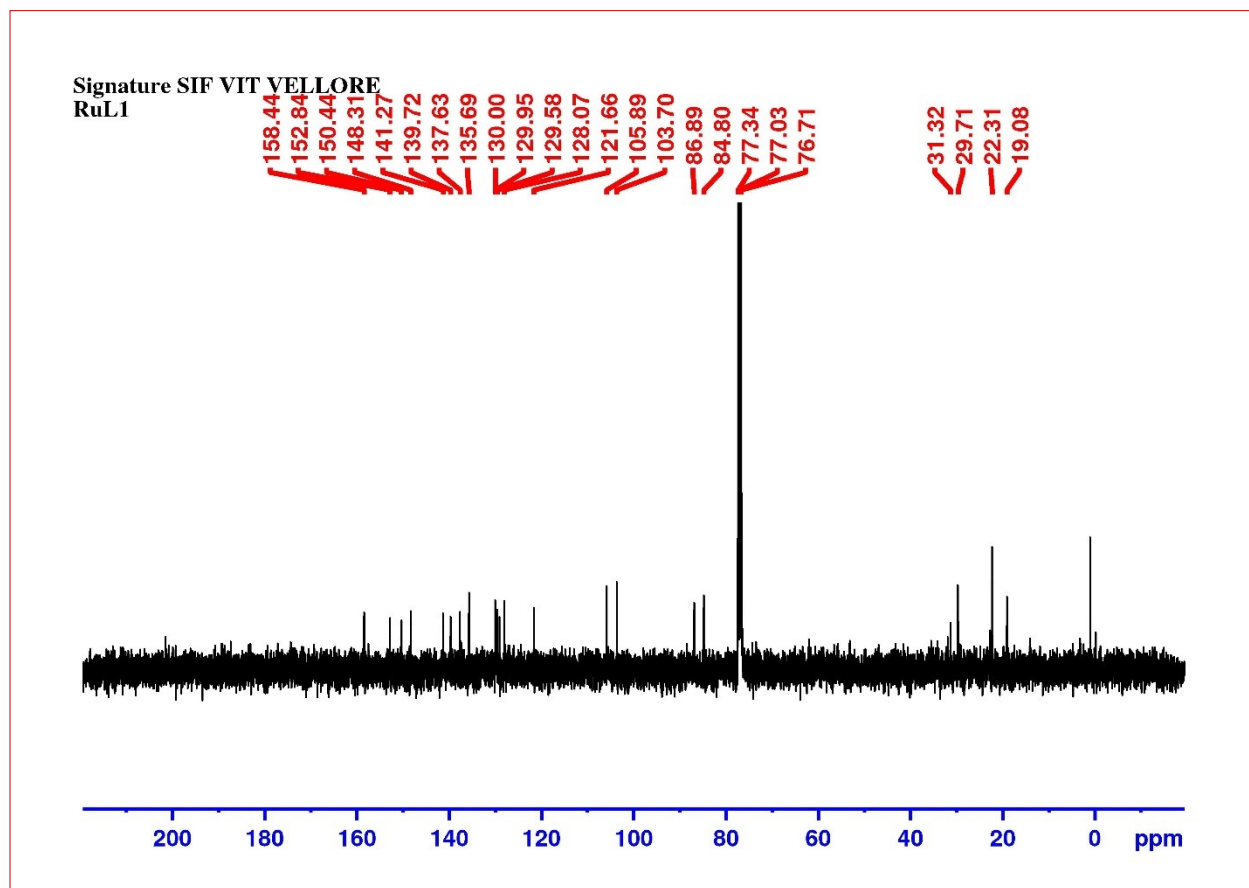
¹H NMR, ¹³C NMR, ¹⁹F NMR,	
³¹P NMR Spectra, ESI-MS	2 - 26
Figure S1-S6	27 - 40

CHARACTERIZATION OF COMPLEXES (RuL1-RuL5):

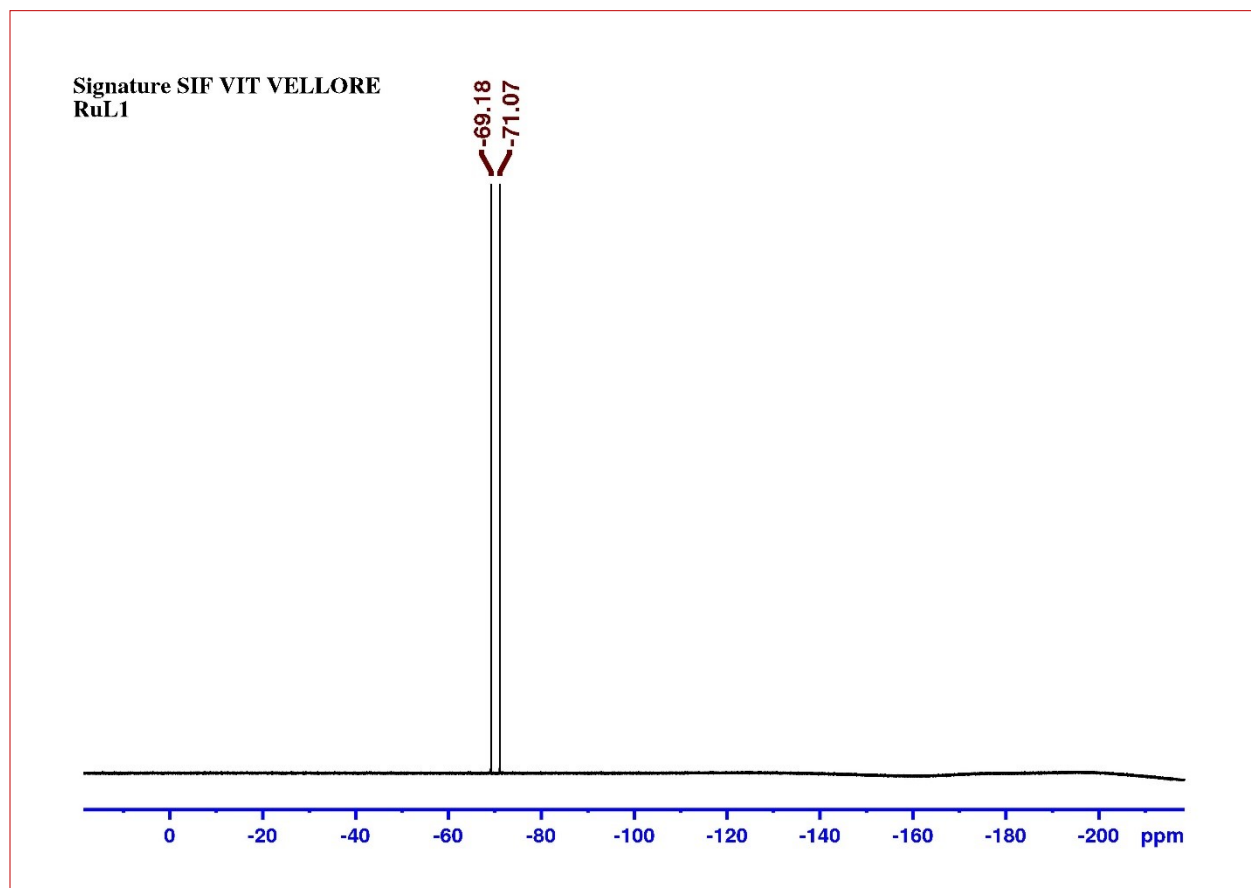
¹H NMR of complex RuL1:



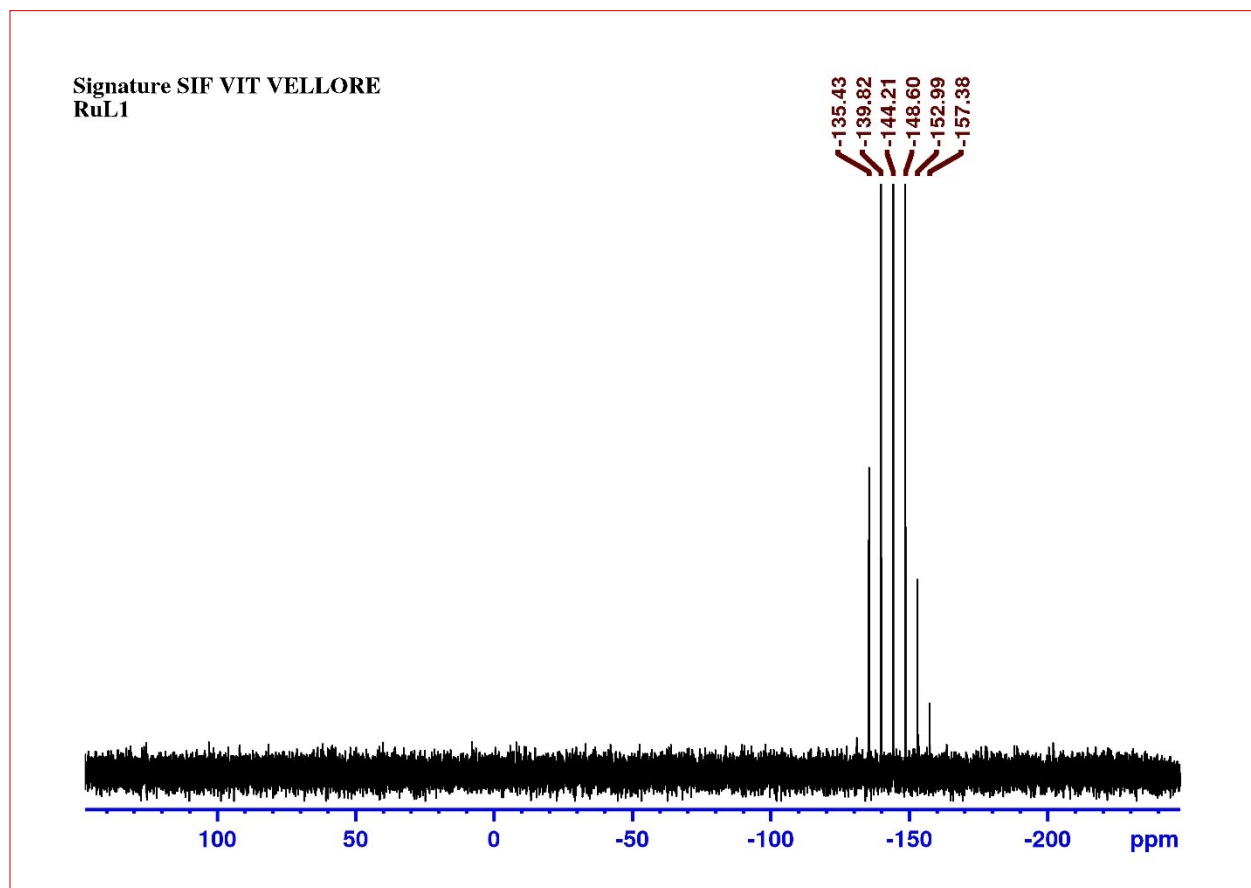
^{13}C NMR of complex RuL1:



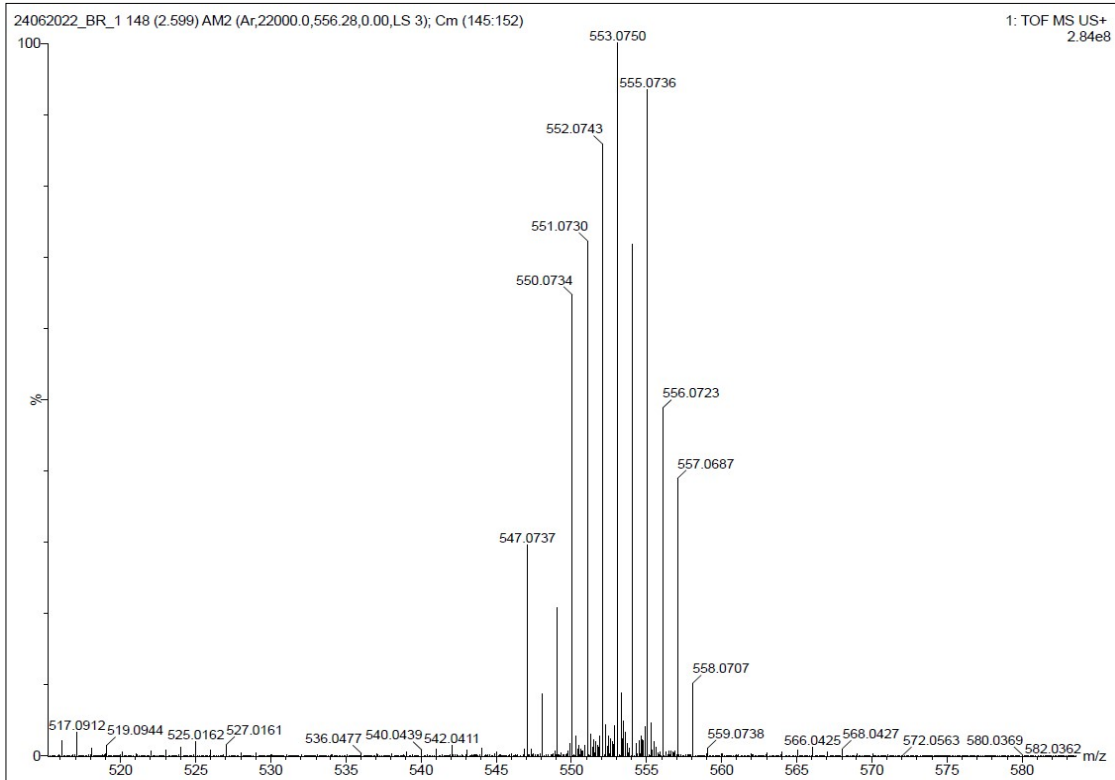
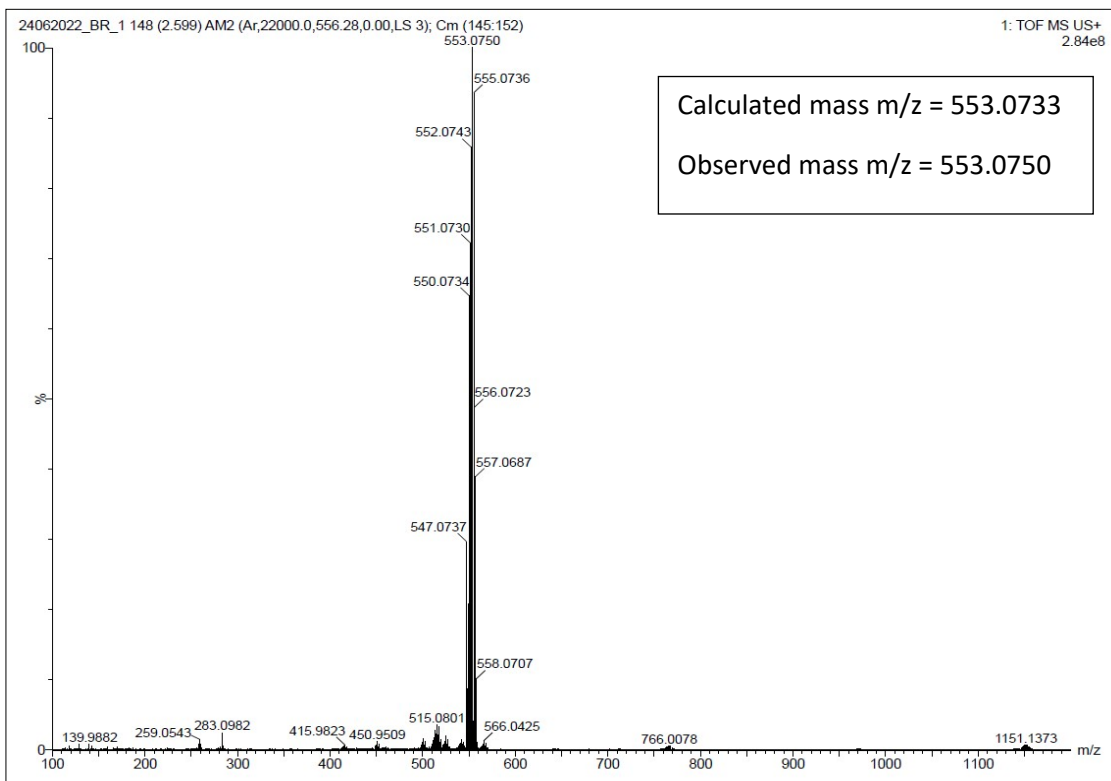
¹⁹F NMR of complex RuL1:



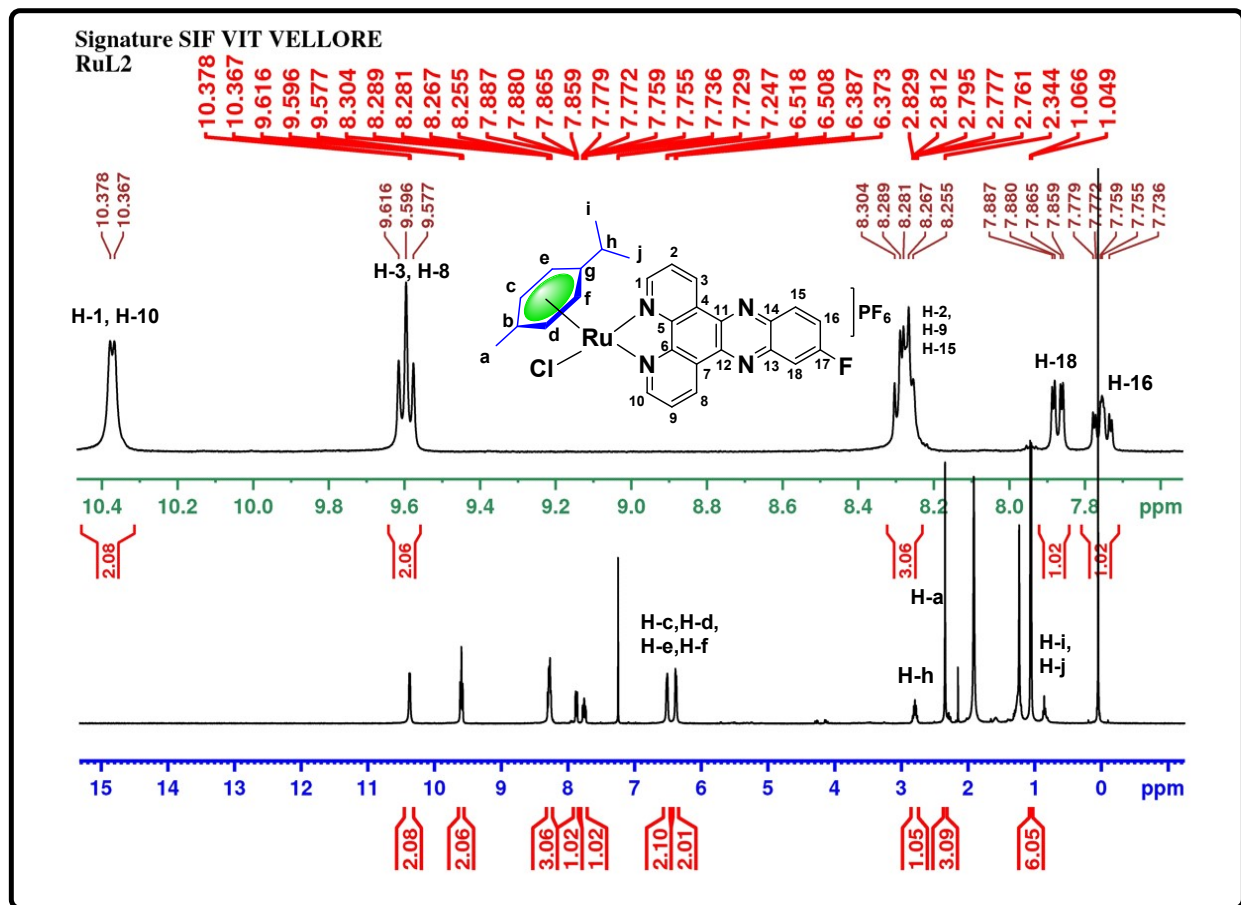
^{31}P NMR of complex RuL1:



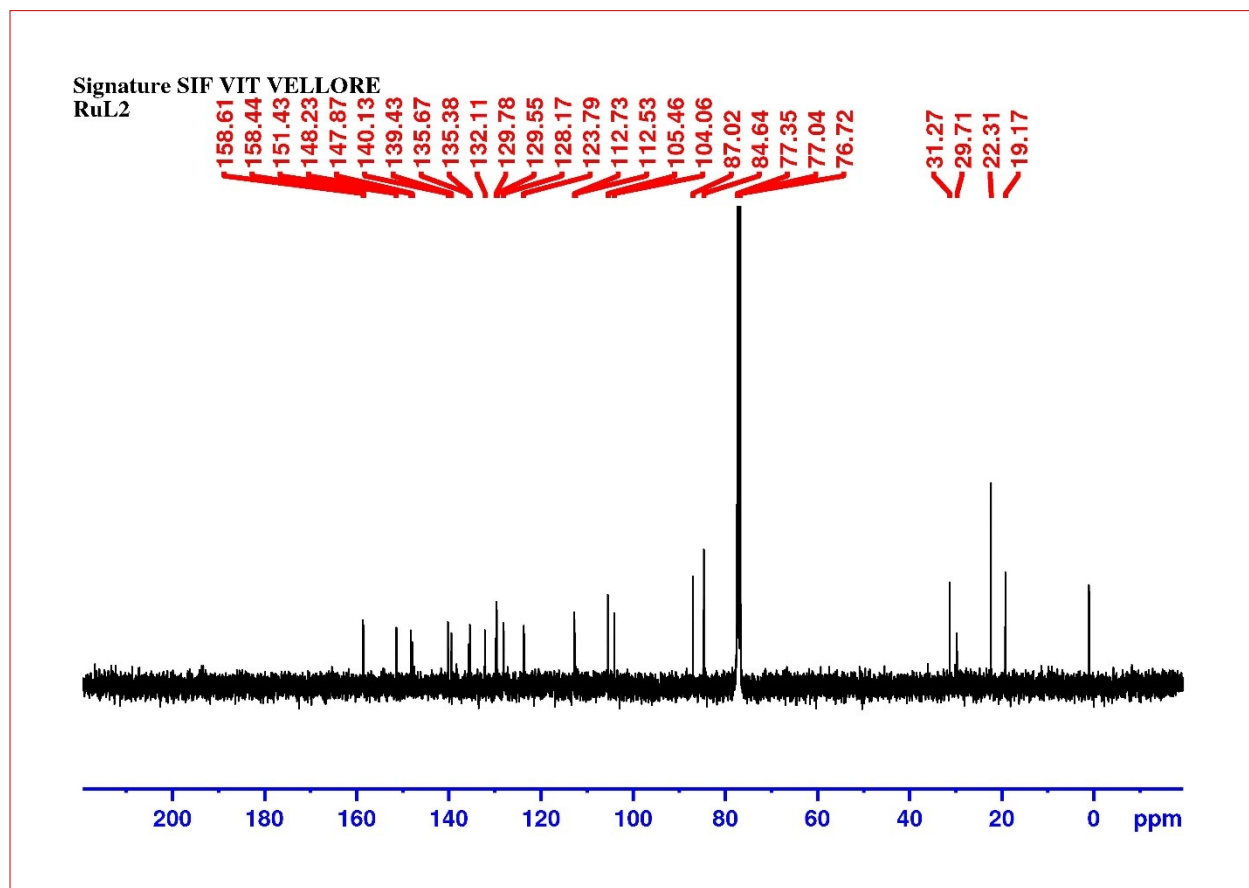
HRMS spectrum of complex RuL1:



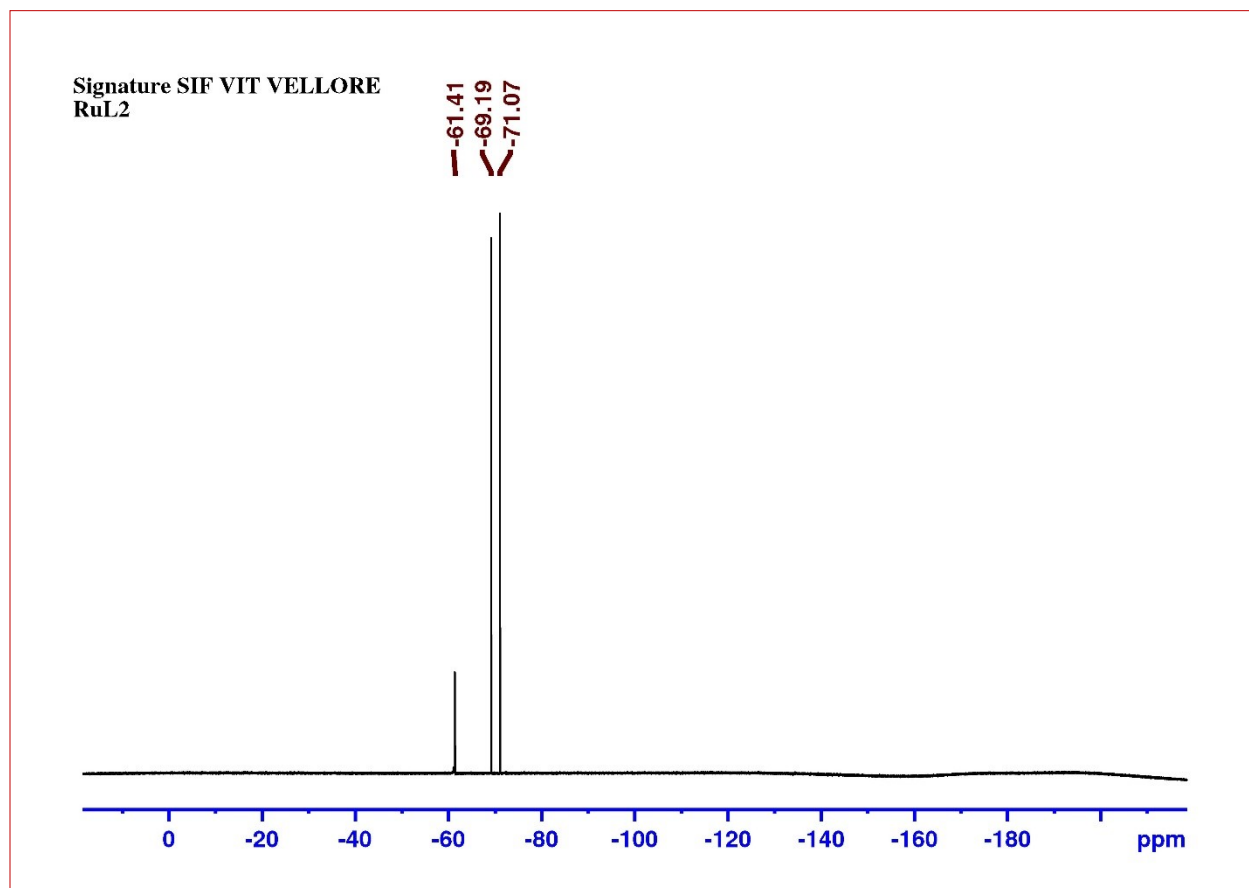
¹H NMR of complex RuL2:



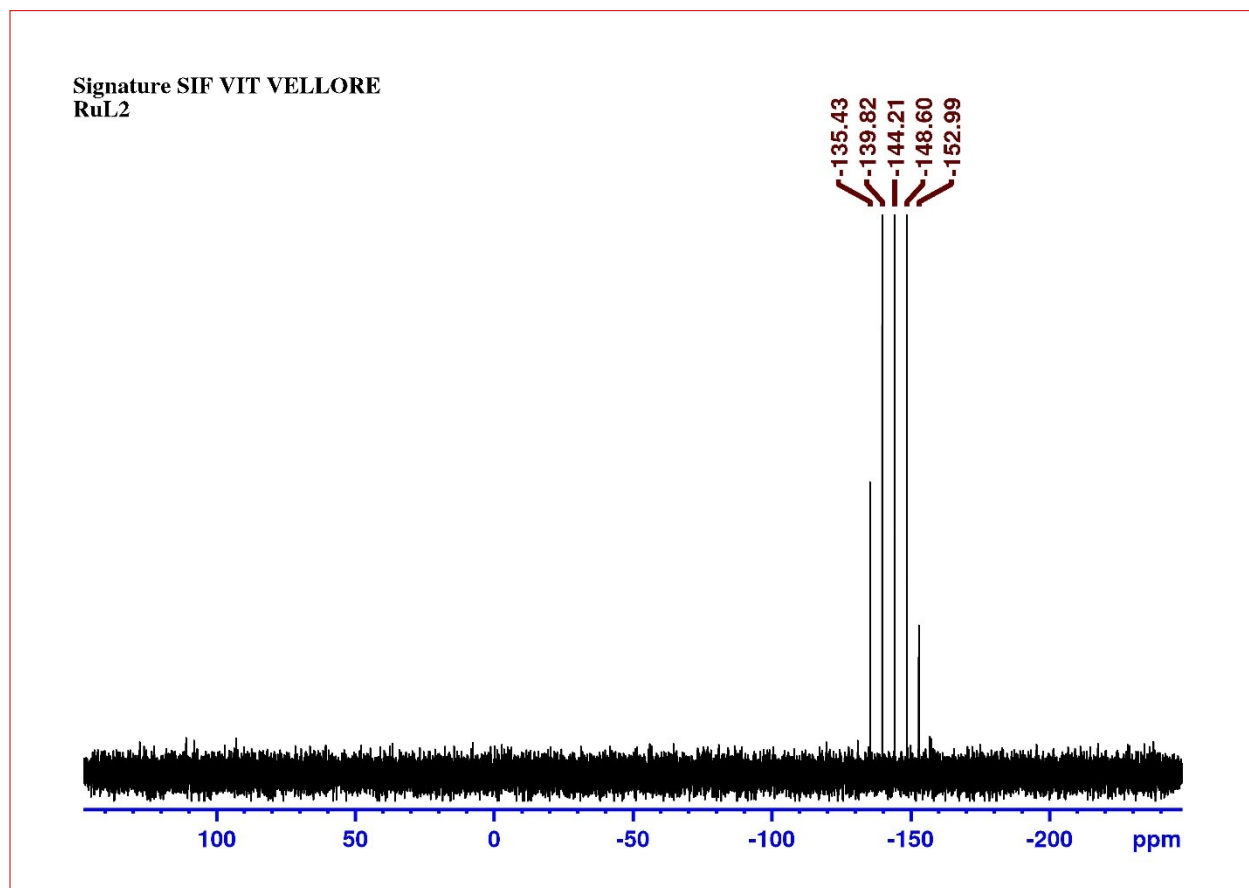
^{13}C NMR of complex RuL2:



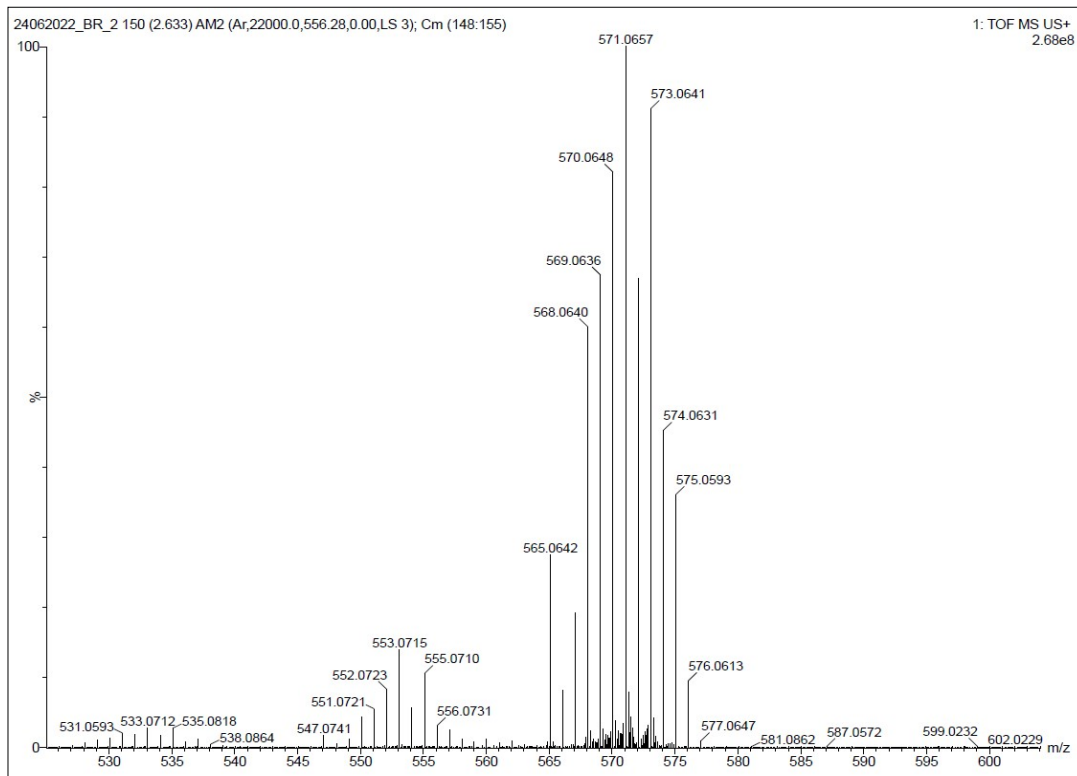
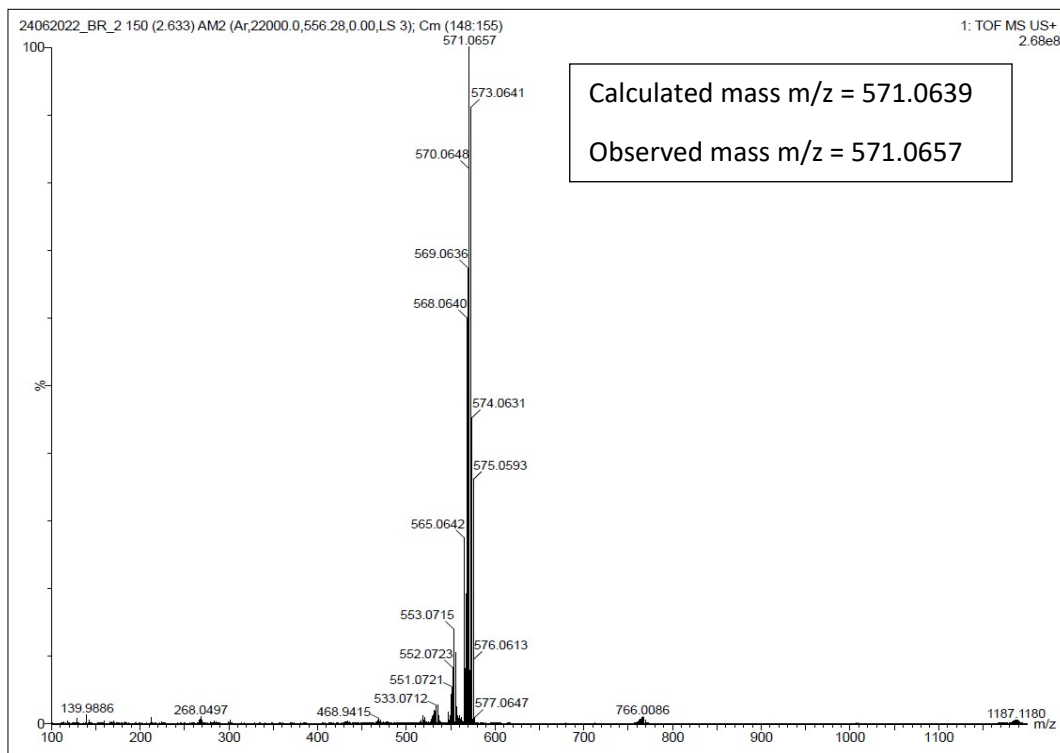
¹⁹F NMR of complex RuL2:



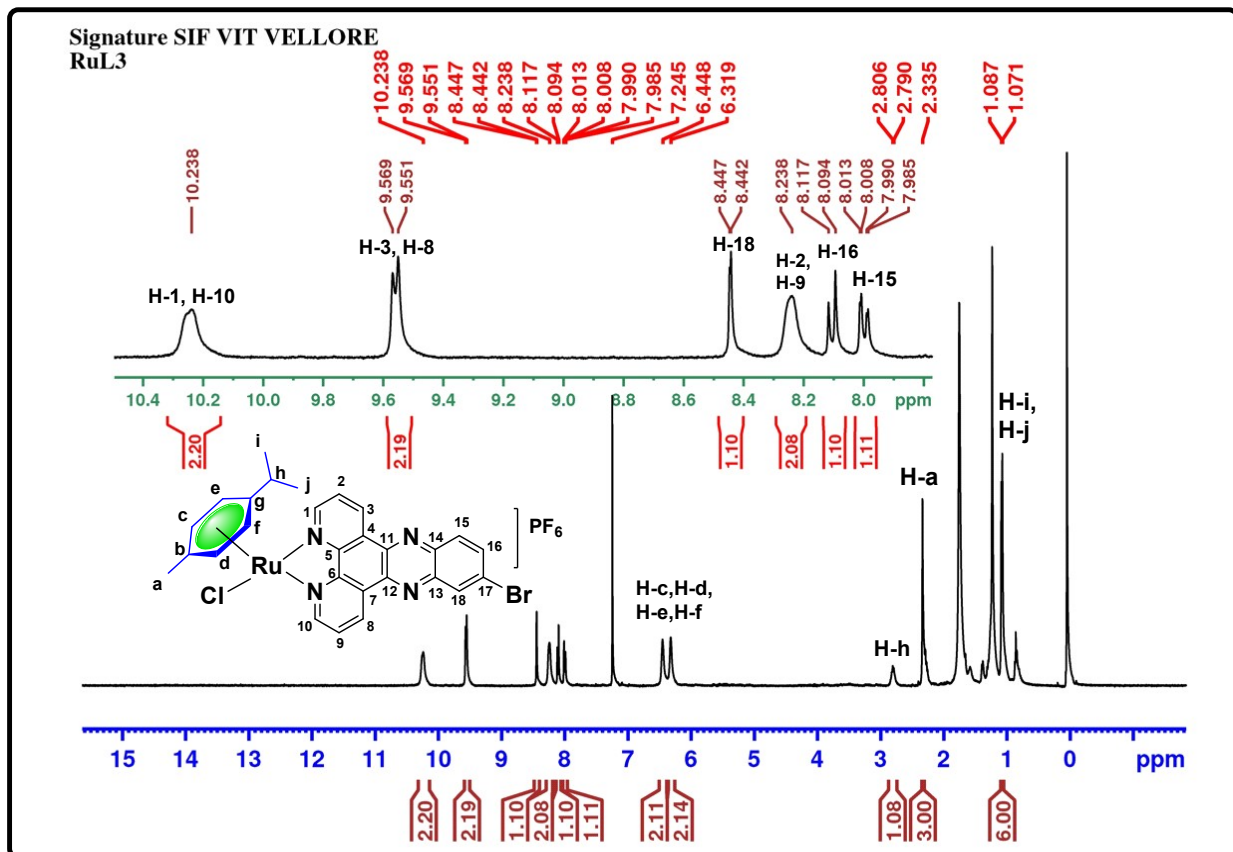
^{31}P NMR of complex RuL2:



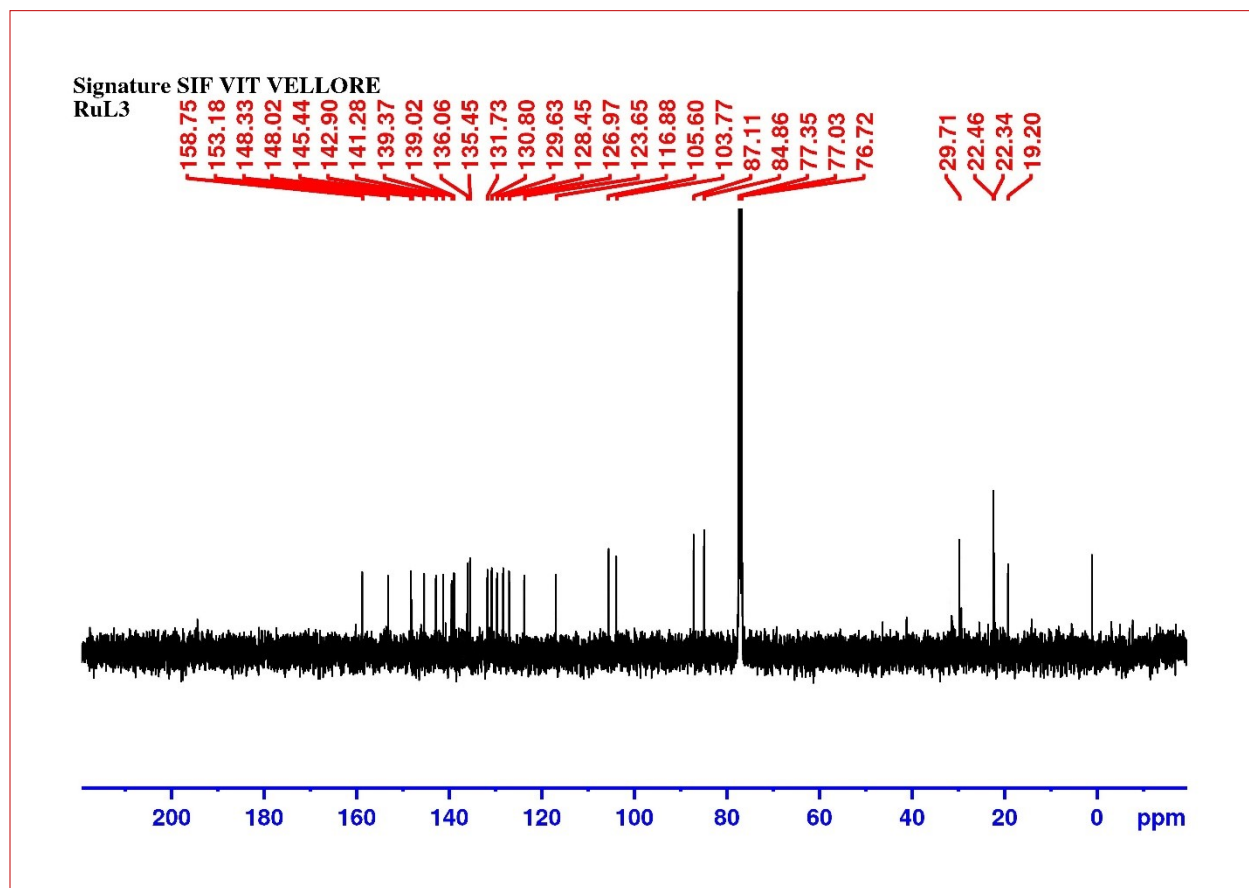
HRMS spectrum of complex RuL2:



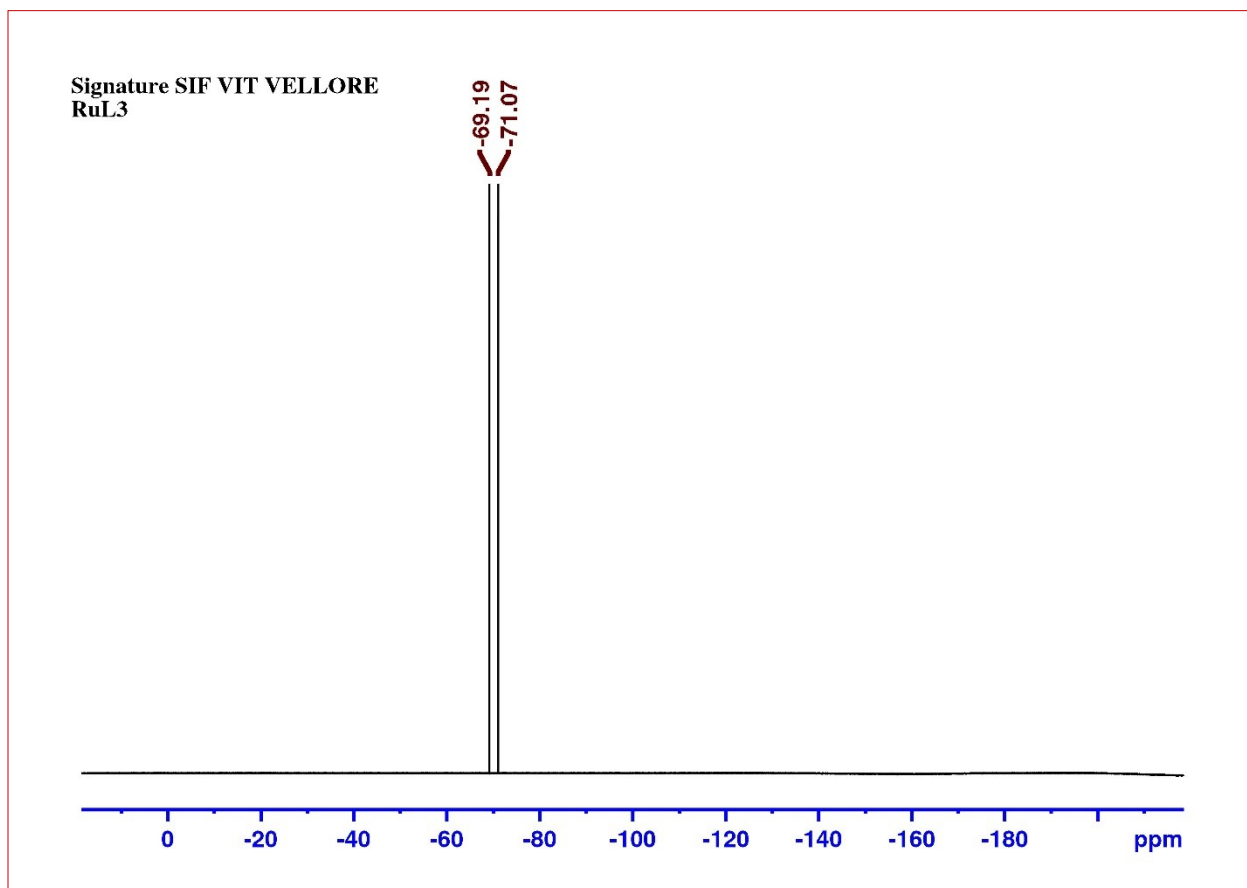
¹H NMR of complex RuL3:



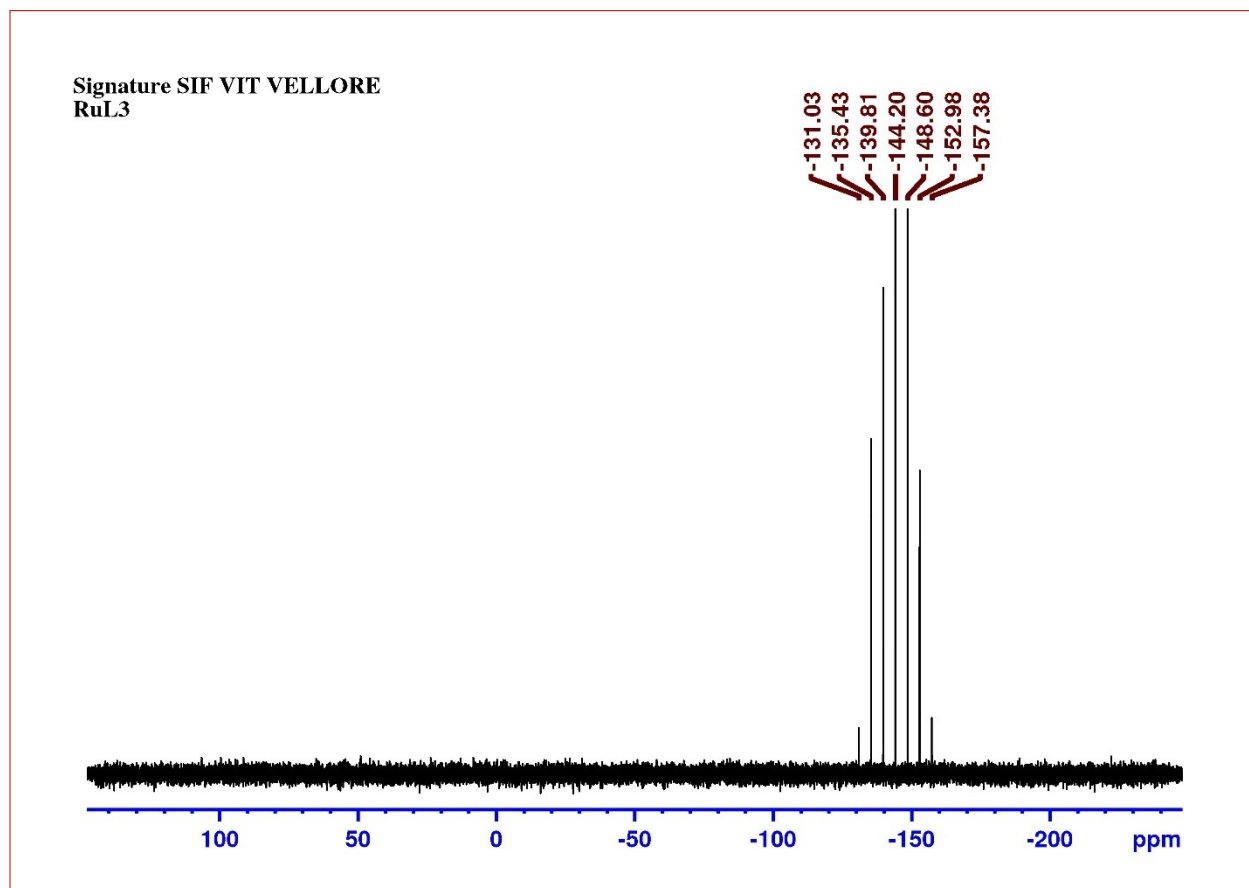
¹³C NMR of complex RuL3:



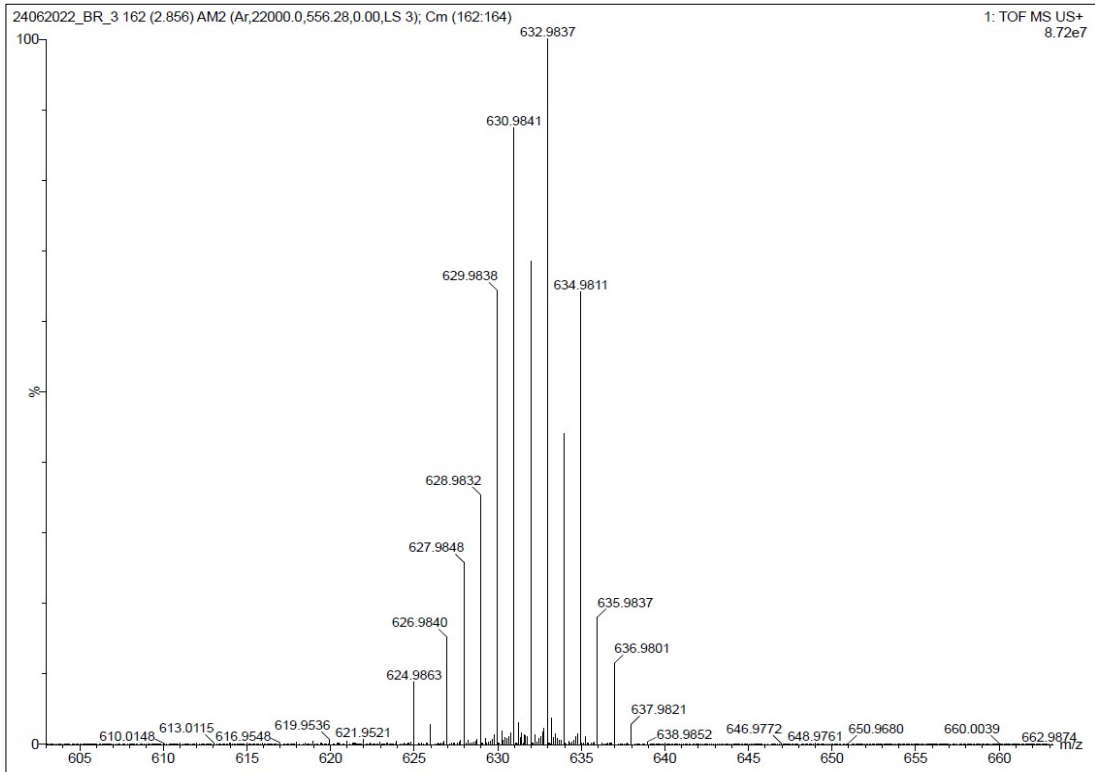
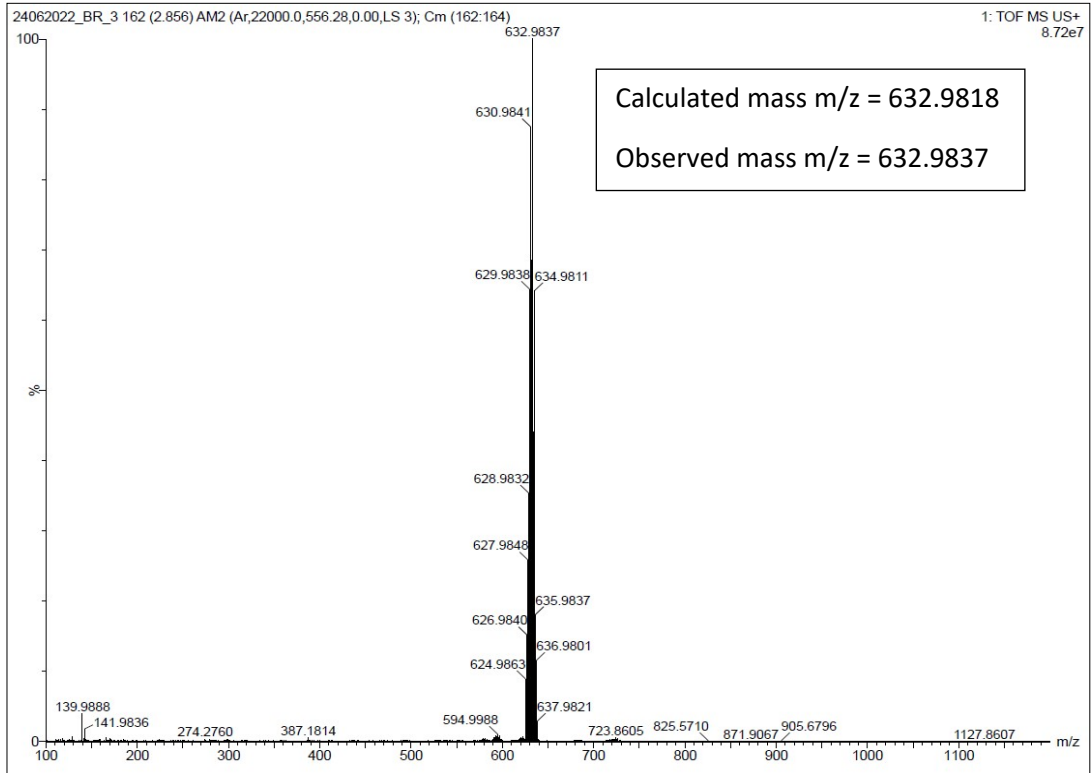
¹⁹F NMR of complex RuL3:



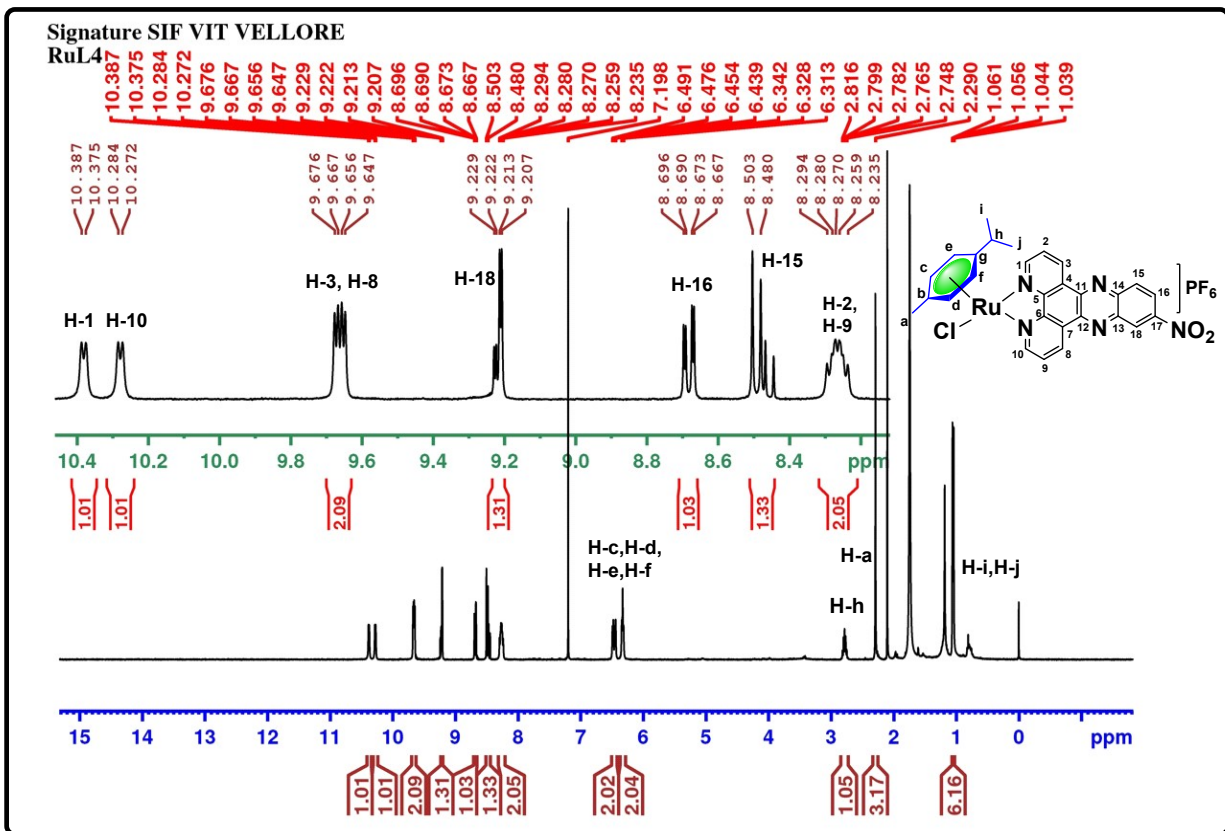
^{31}P NMR of complex RuL3:



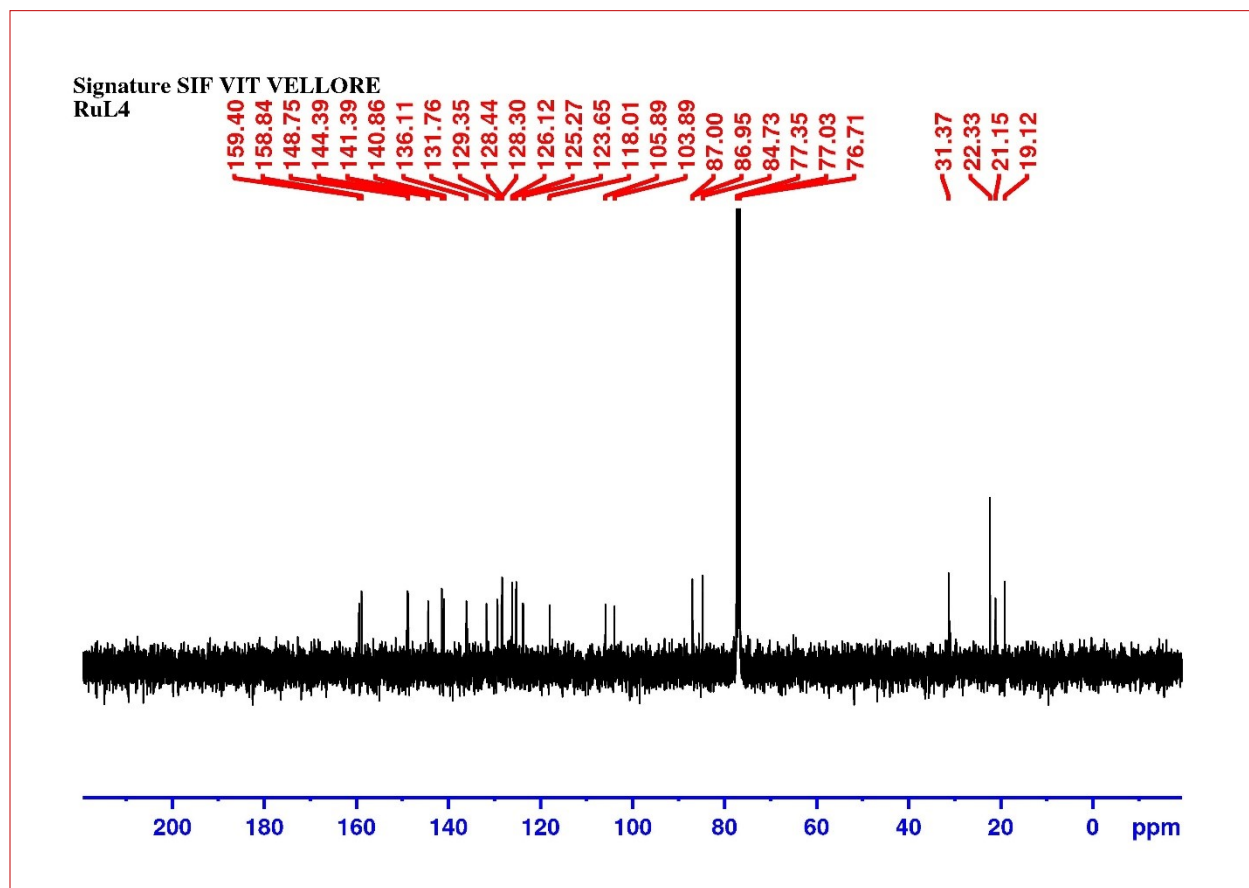
HRMS spectrum of complex RuL3:



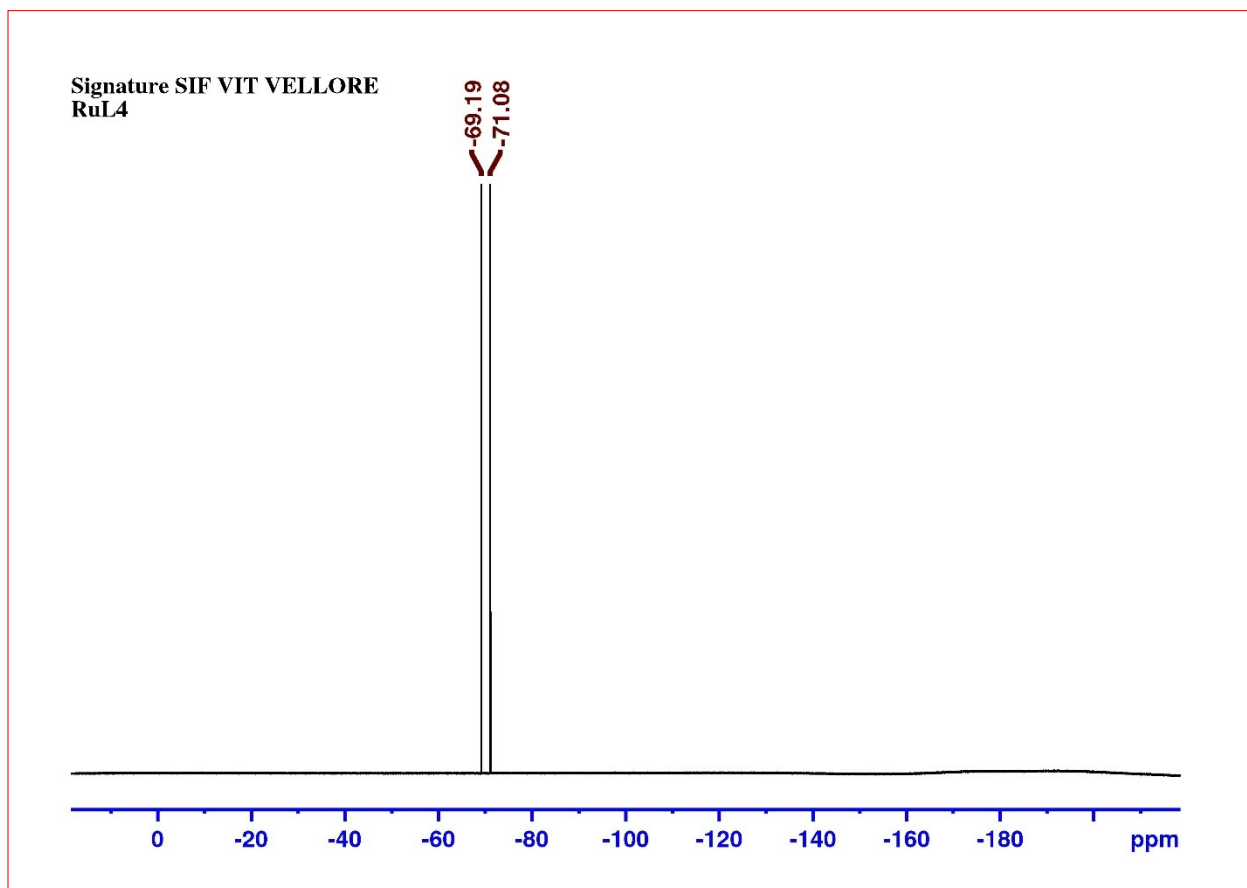
¹H NMR of complex RuL4:



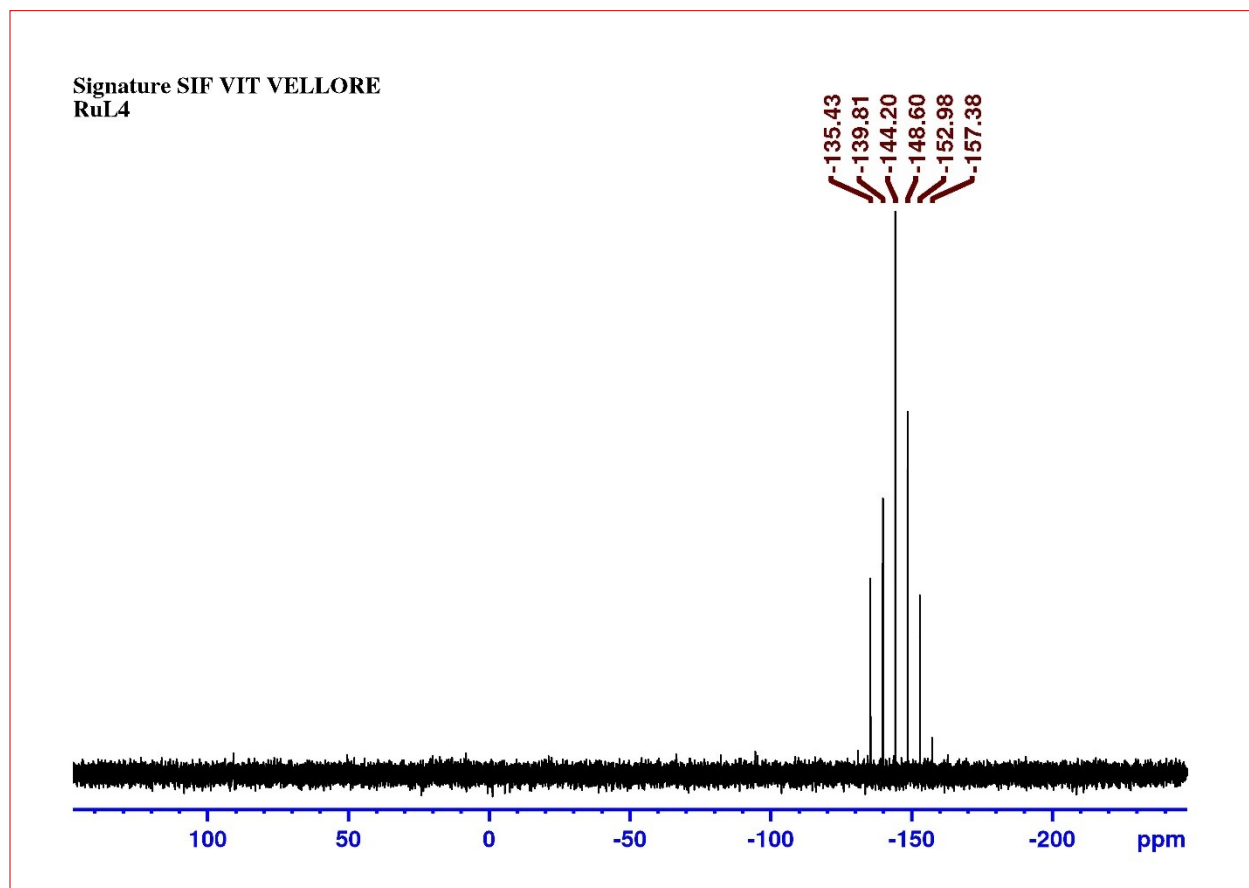
¹³C NMR of complex RuL4:



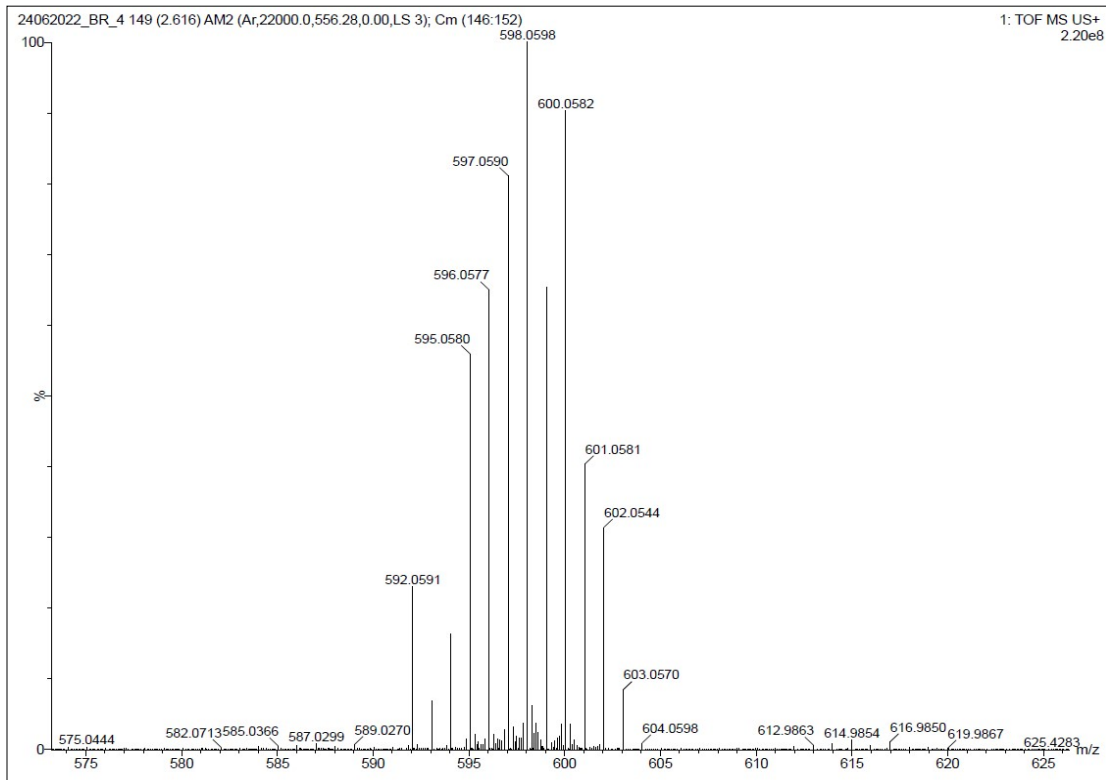
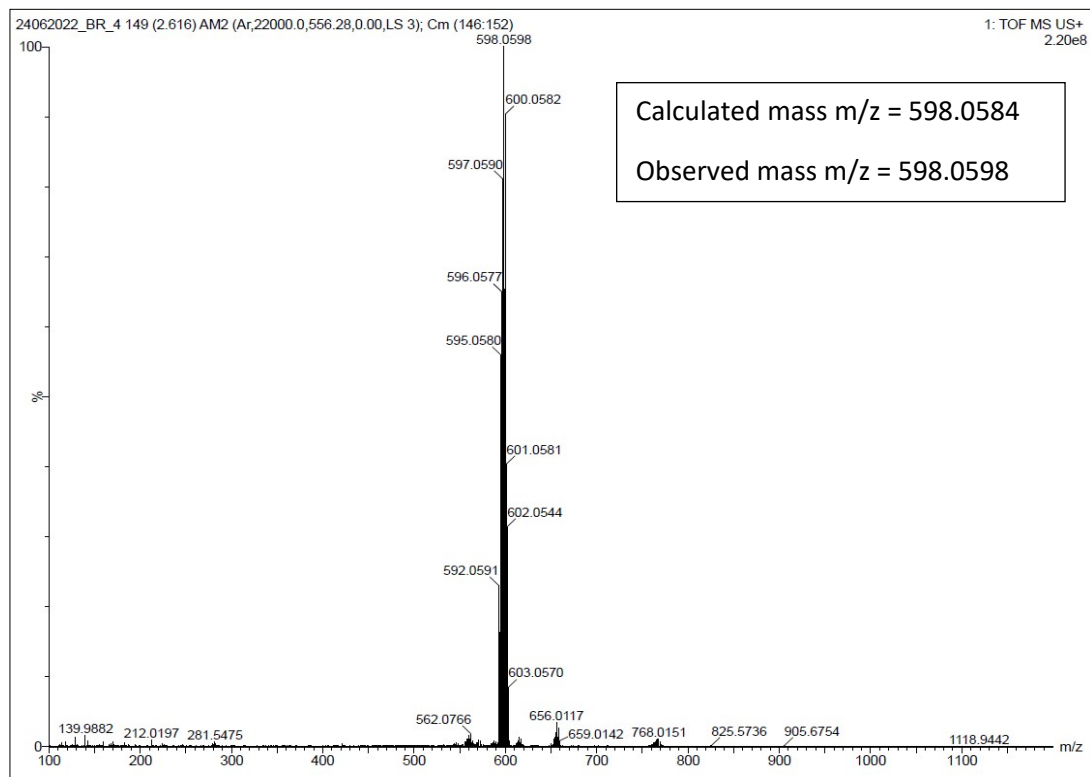
^{19}F NMR of complex RuL4:



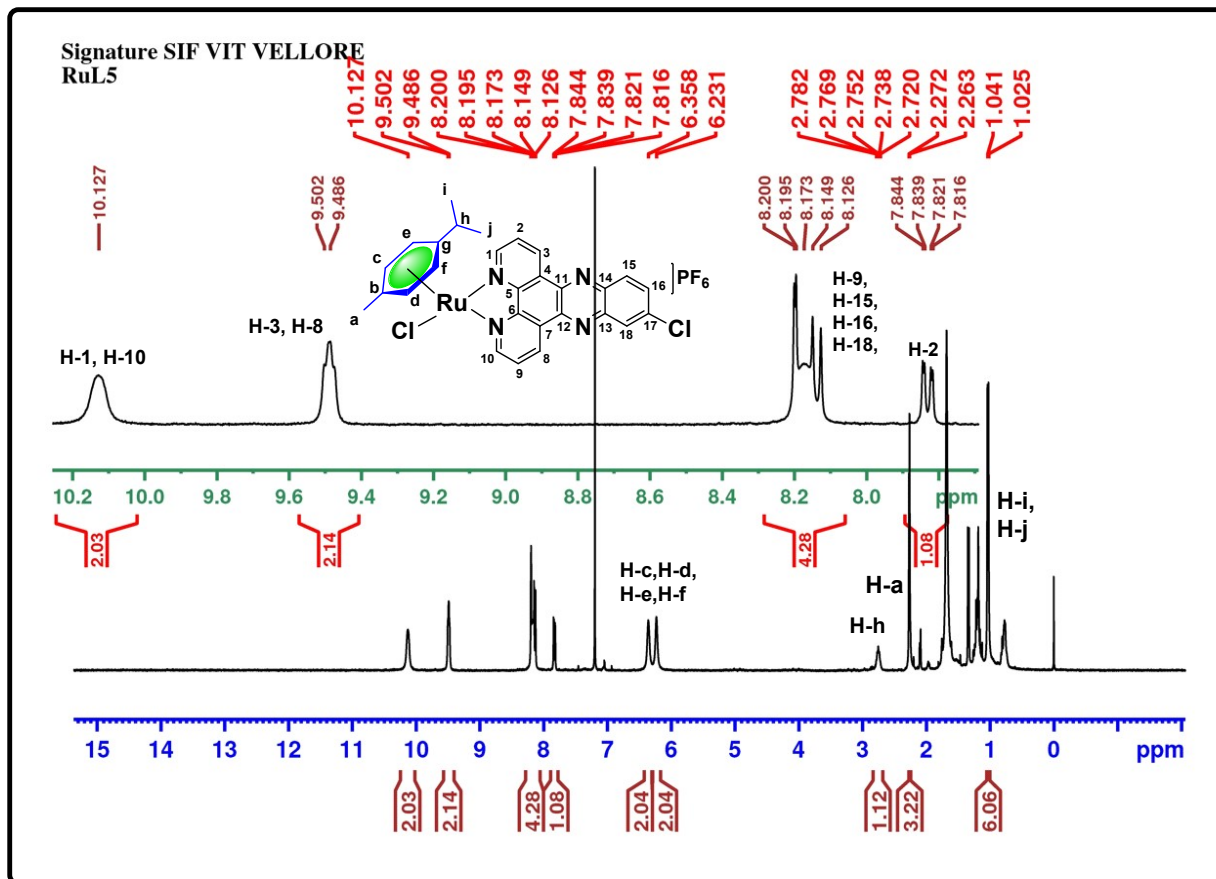
^{31}P NMR of complex RuL4:



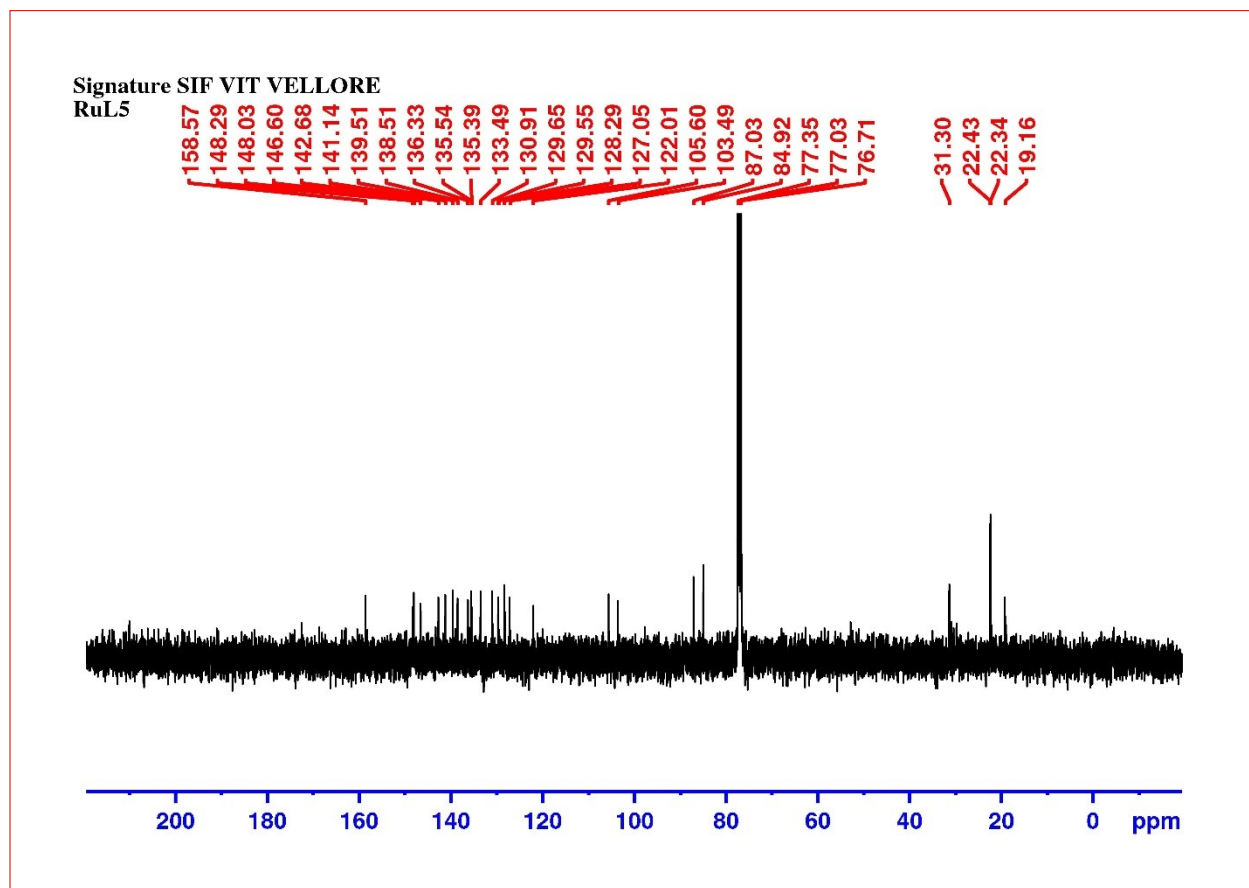
HRMS spectrum of complex RuL4:



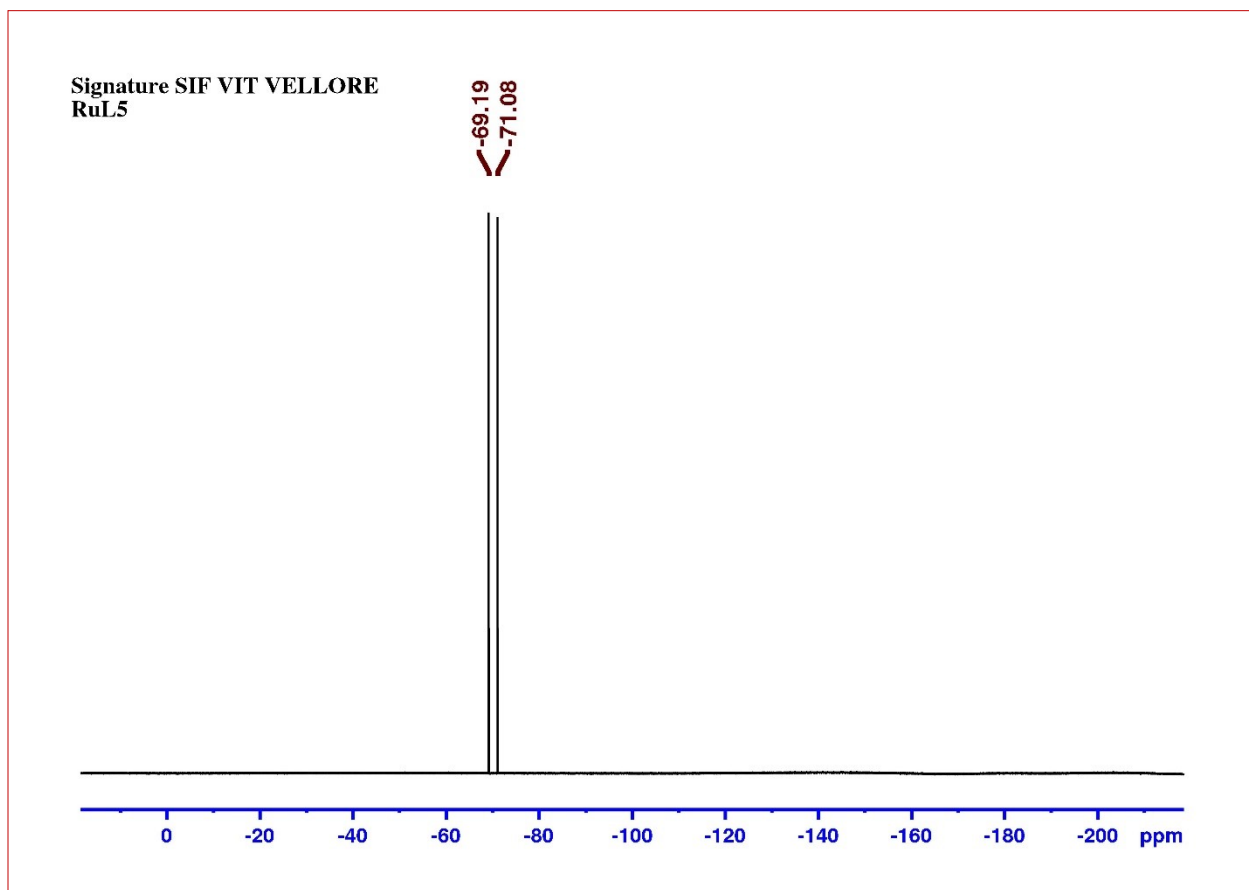
¹H NMR of complex RuL5:



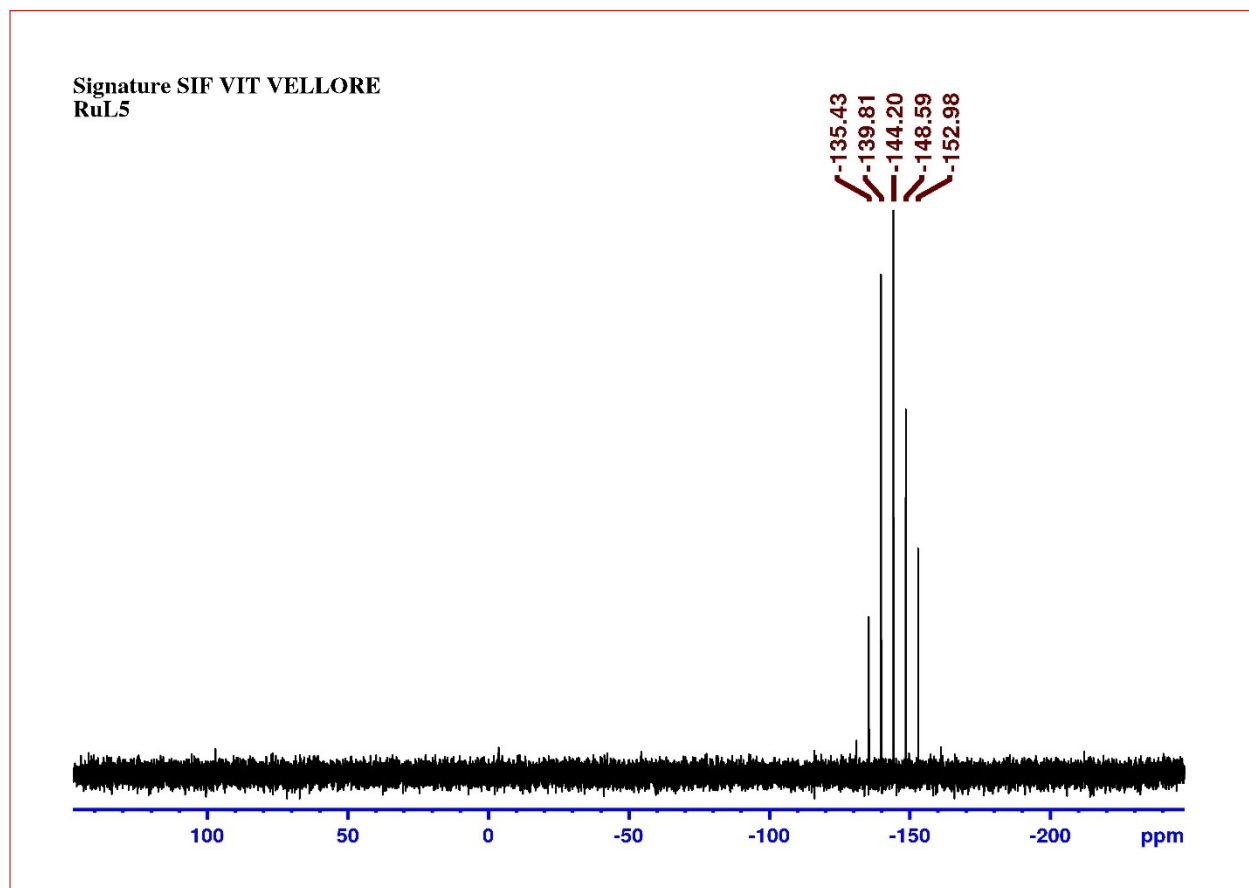
^{13}C NMR of complex RuL5:



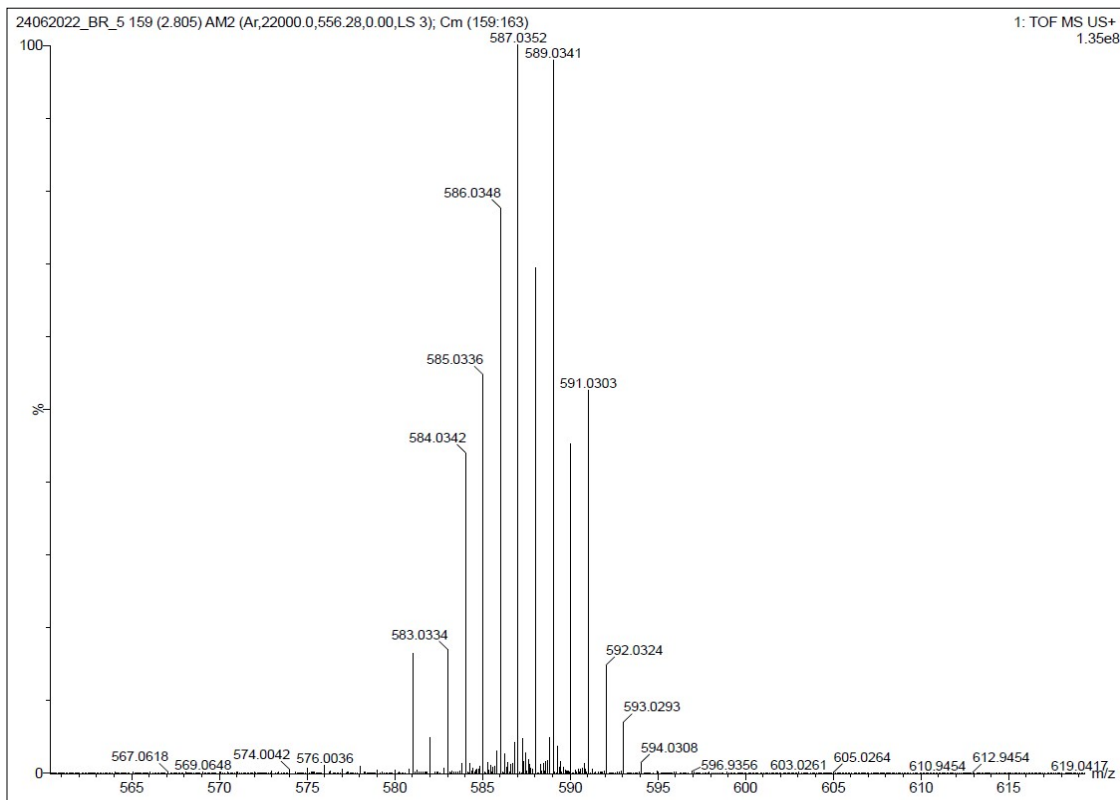
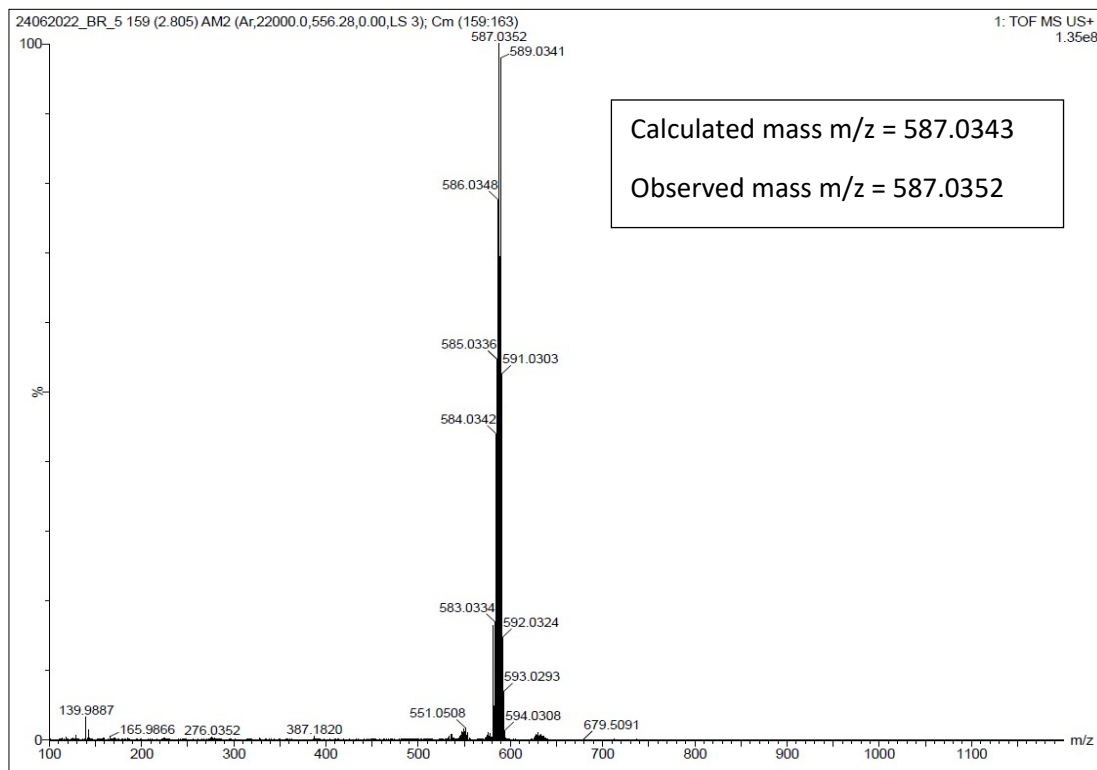
¹⁹F NMR of complex RuL5:



^{31}P NMR of complex RuL5:



HRMS spectrum of complex RuL5:



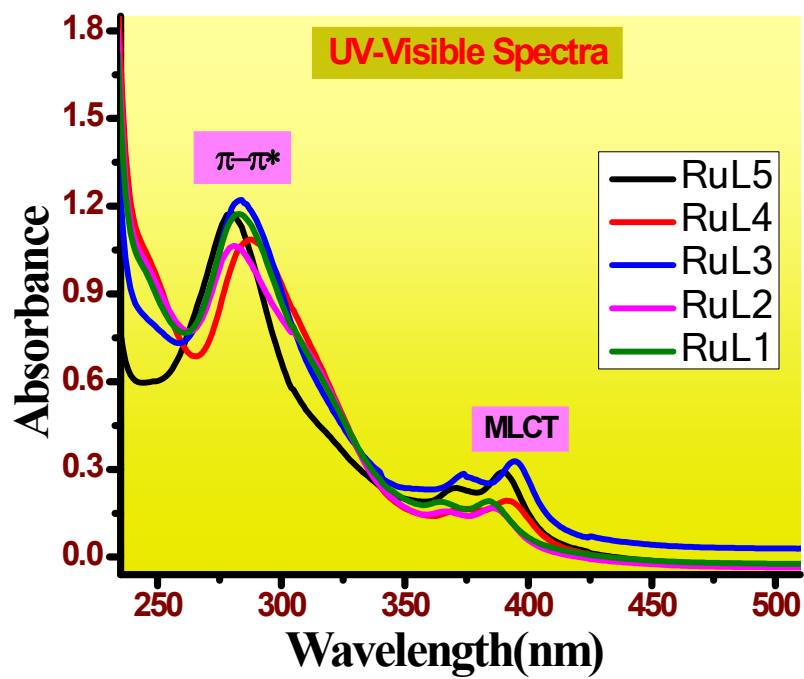


Fig. S1: Absorption spectra of complexes RuL1-RuL5 in 10% DMSO solutions (3×10^{-5} M)

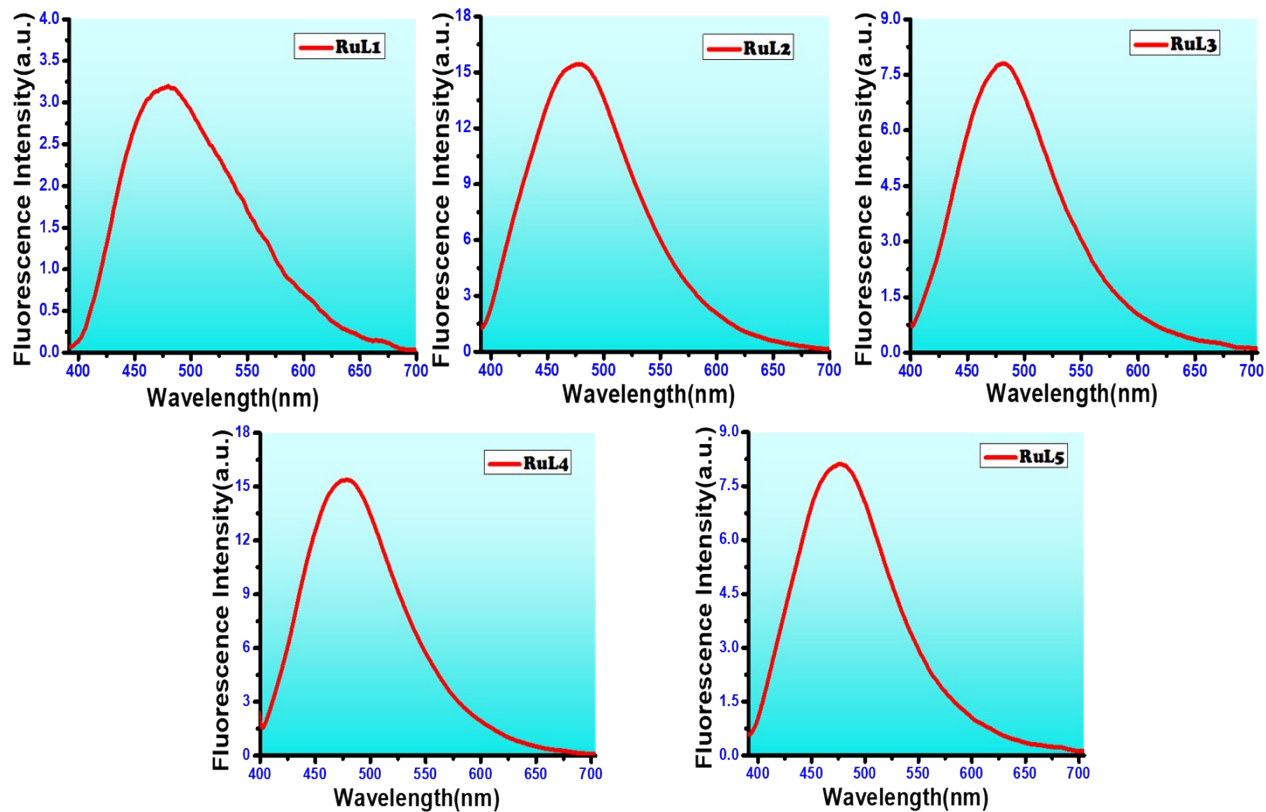


Fig. S2: Emission spectra of complexes RuL1–RuL5 in 10% DMSO-water (concentration = 3×10^{-5} M, $\lambda_{ex} = 300$ nm).

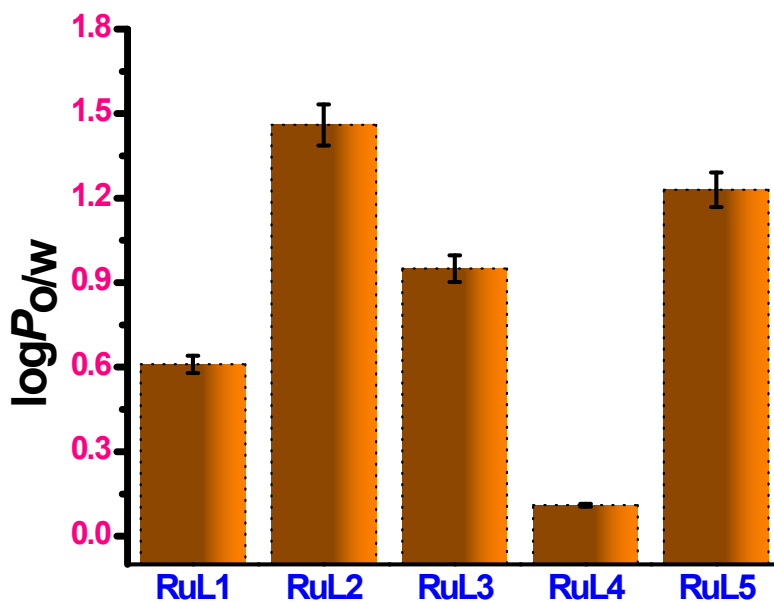


Fig. S3: Representative diagram of lipophilicity of RuL1–RuL5 showed by a bar diagram displaying comparative $\log P_{o/w}$ values of complexes in Octanol–water system, where error bars in the graph specify the standard deviation in measurement.

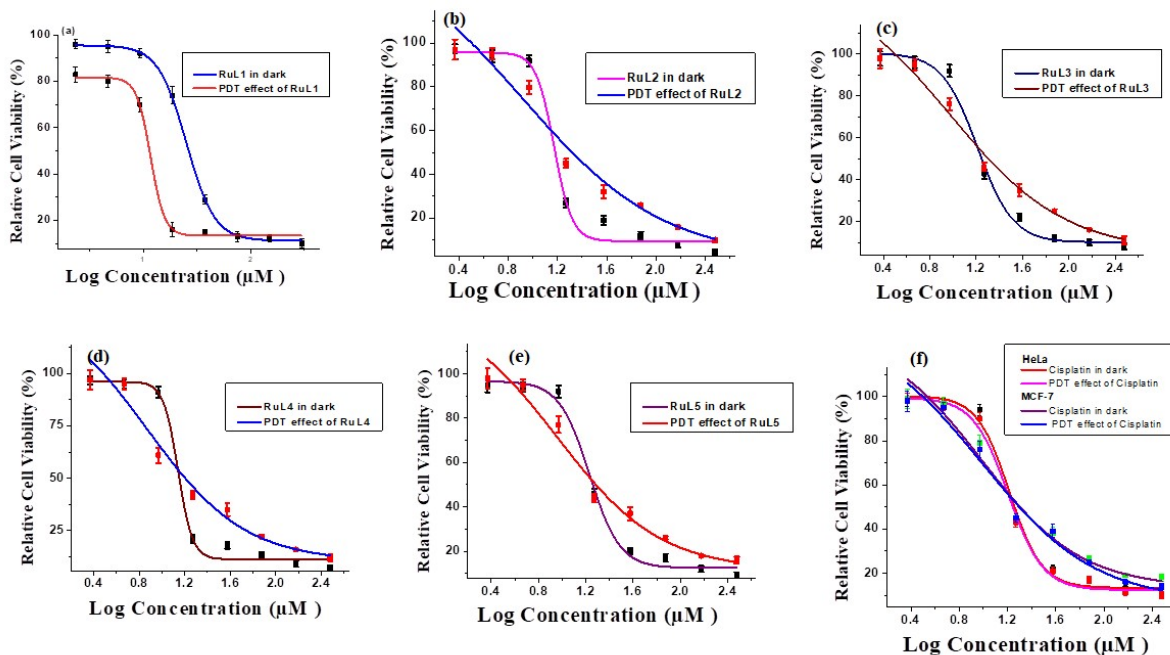


Fig. S4: Cytotoxicity study of (a-e) complex RuL1-RuL5 against HeLa cell line under dark and in presence of light (f) Cisplatin against HeLa and MCF-7 cell line under dark and in presence of light

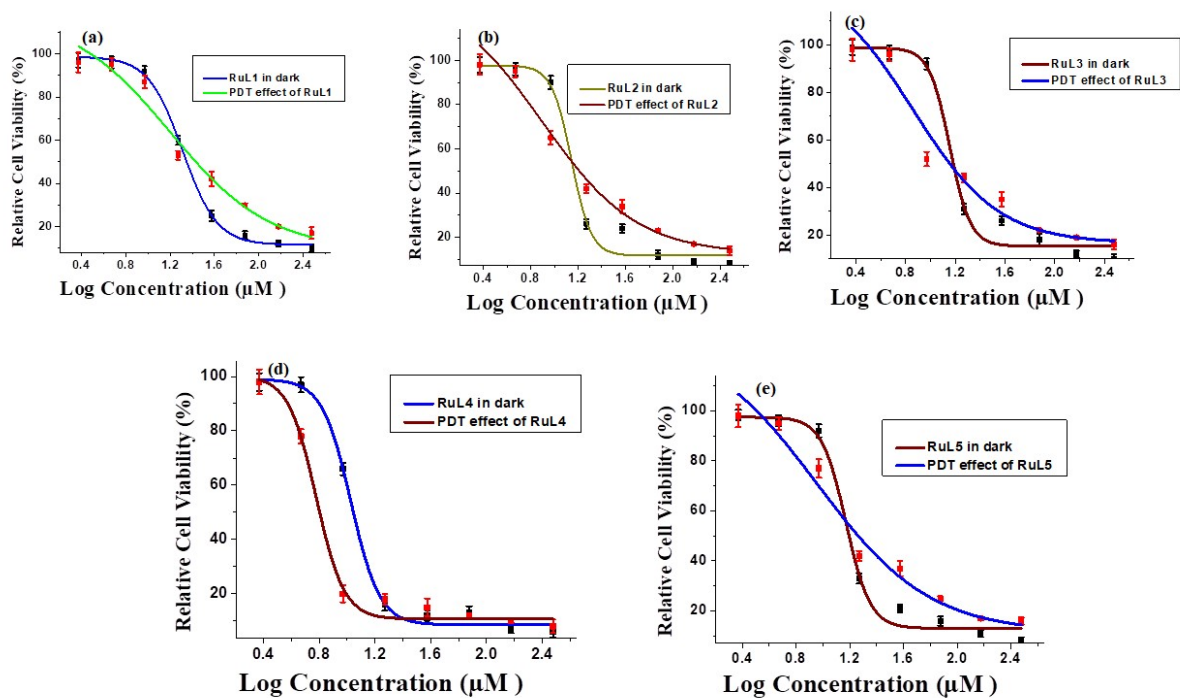
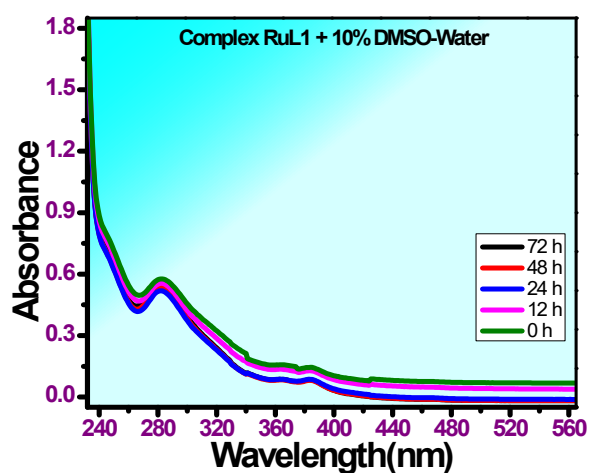
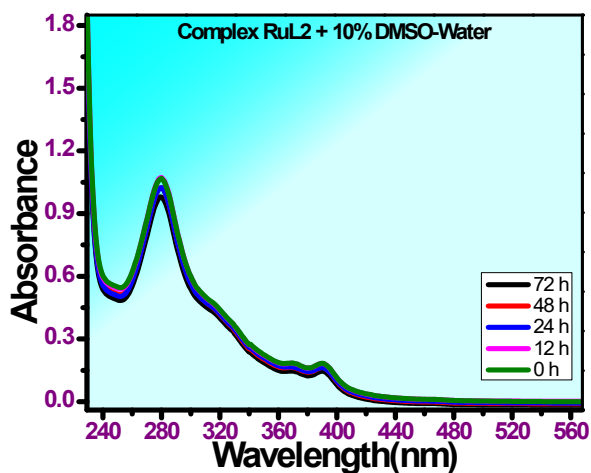


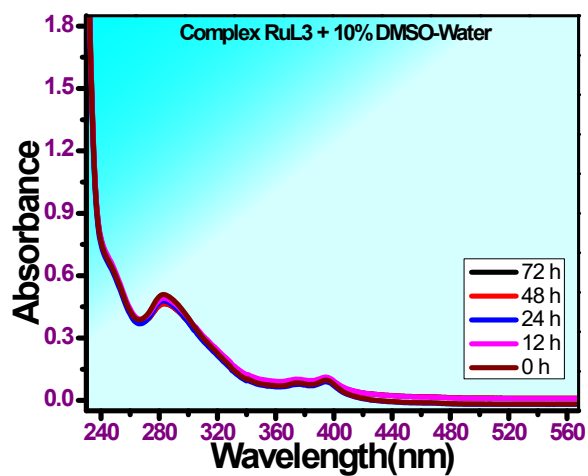
Fig. S5: Cytotoxicity study of (a-e) complex RuL1-RuL5 against MCF-7 cell line under dark and in presence of light



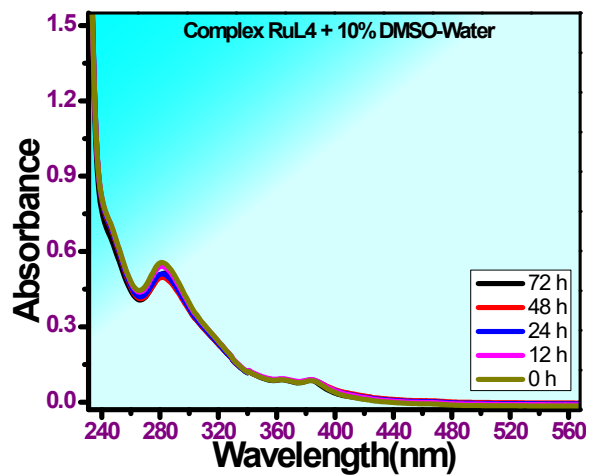
(a)



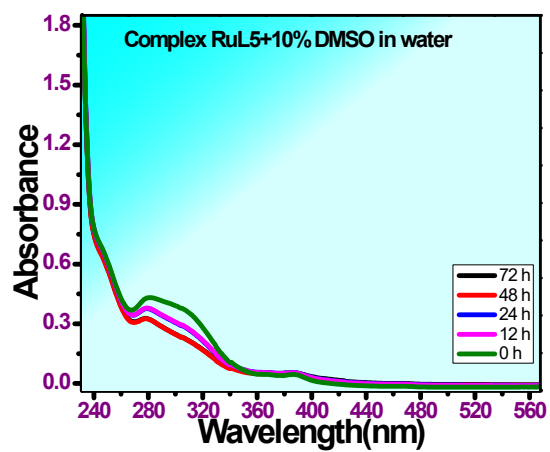
(b)



(c)

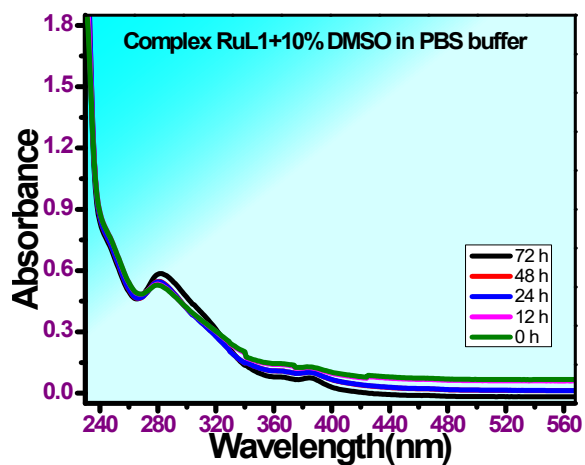


(d)

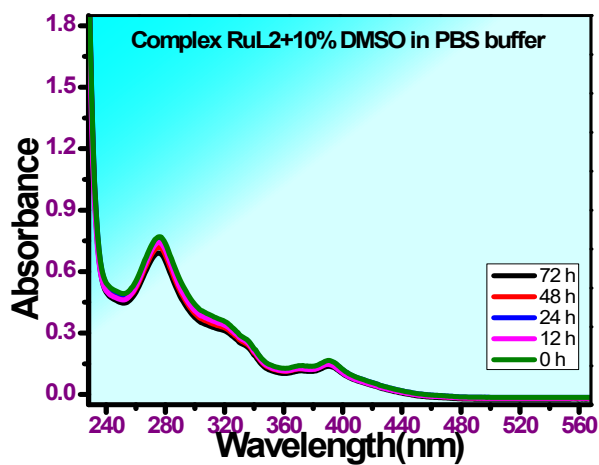


(e)

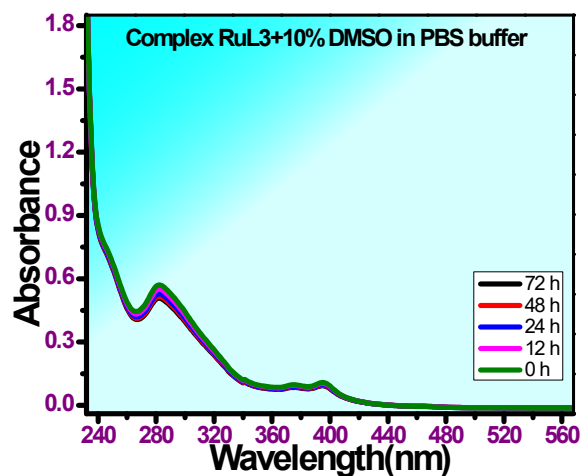
Fig. S6: Stability of all five complexes (RuL1-RuL5) in 10% DMSO media.



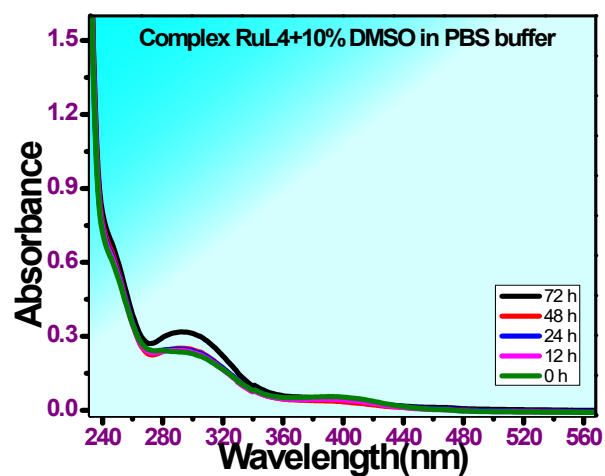
(a)



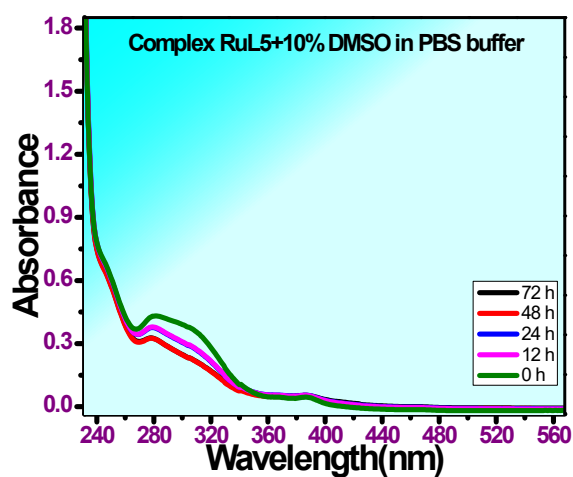
(b)



(c)

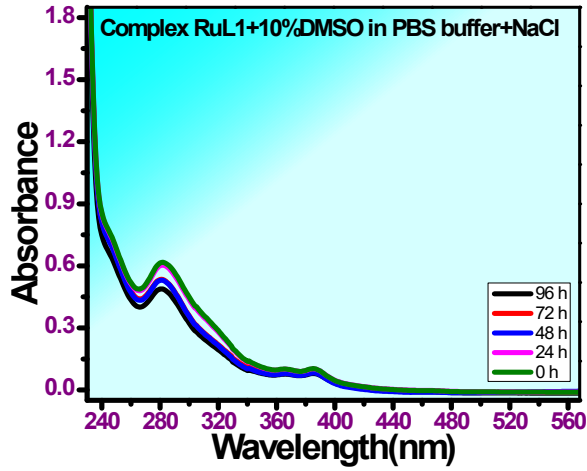


(d)

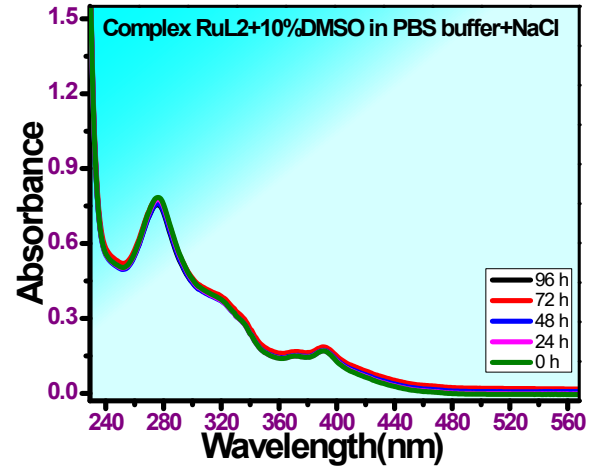


(e)

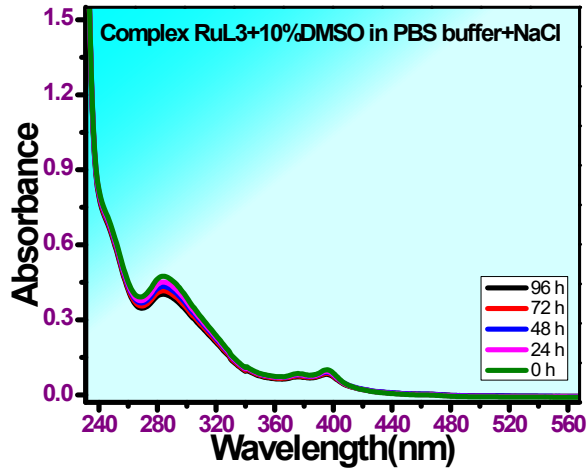
Fig. S7: Stability of all five complexes (RuL1-RuL5) in 10% DMSO-PBS buffer media.



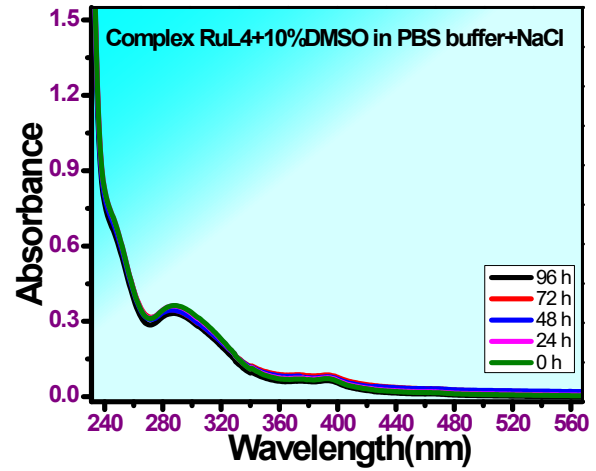
(a)



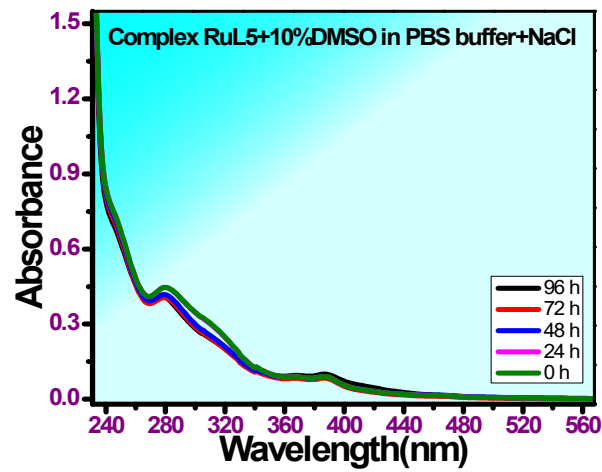
(b)



(c)

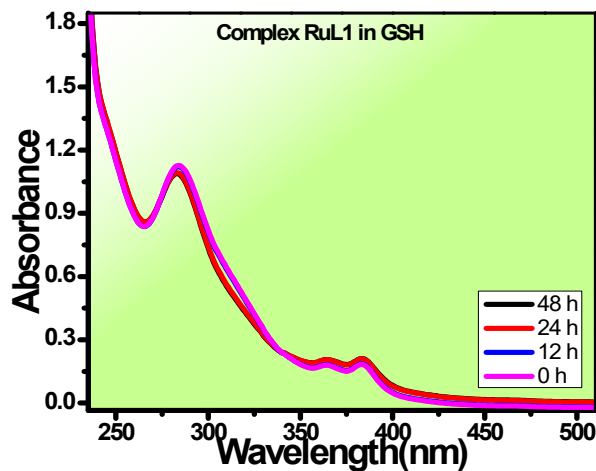


(d)

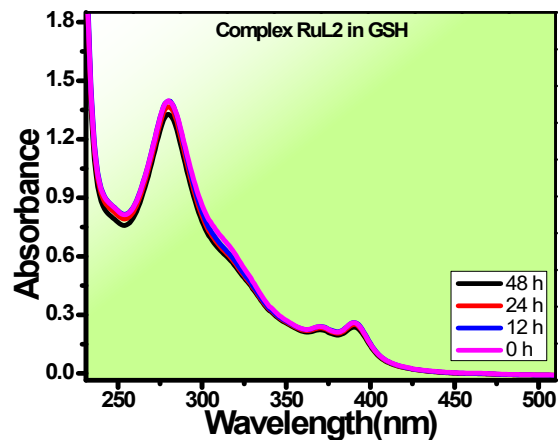


(e)

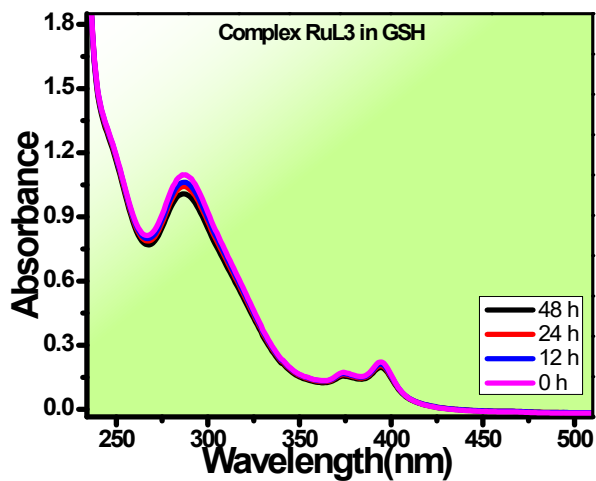
Fig. S8: Stability of all five complexes (RuL1-RuL5) in 10% DMSO-PBS buffer media in presence of NaCl.



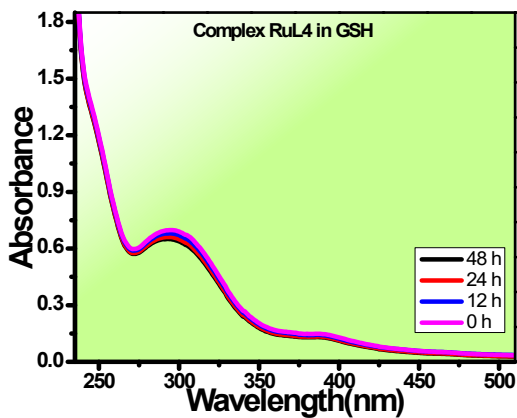
(a)



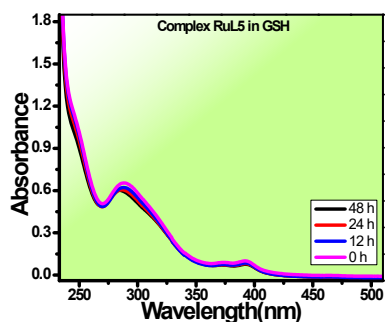
(b)



(c)



(d)



(e)

Fig. S9: Stability of all five complexes (RuL1-RuL5) in 1mM 1mM GSH media

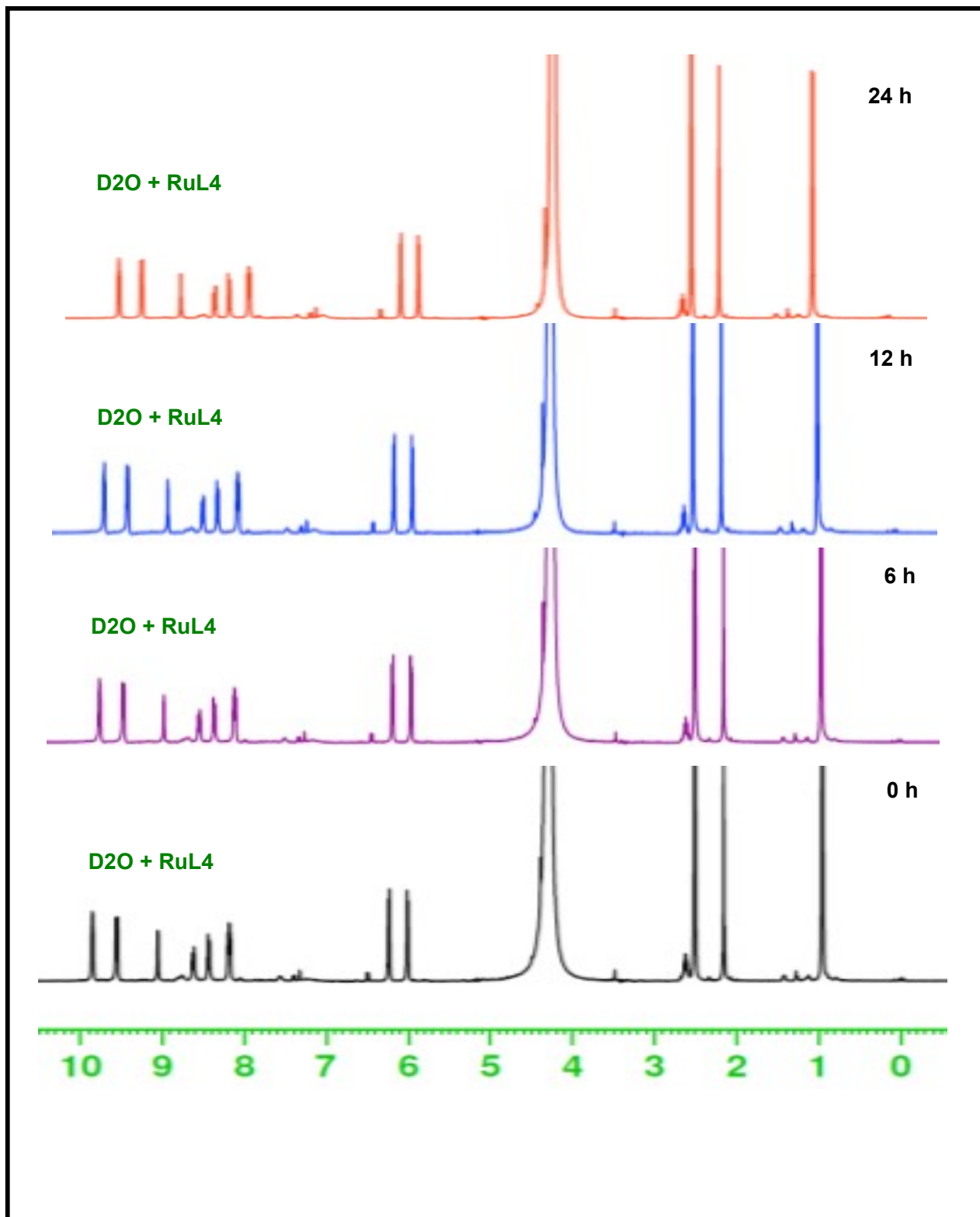


Fig. S10 Stability study of complex **RuL4** in presence of DMSO-D₂O *via* ¹H NMR.

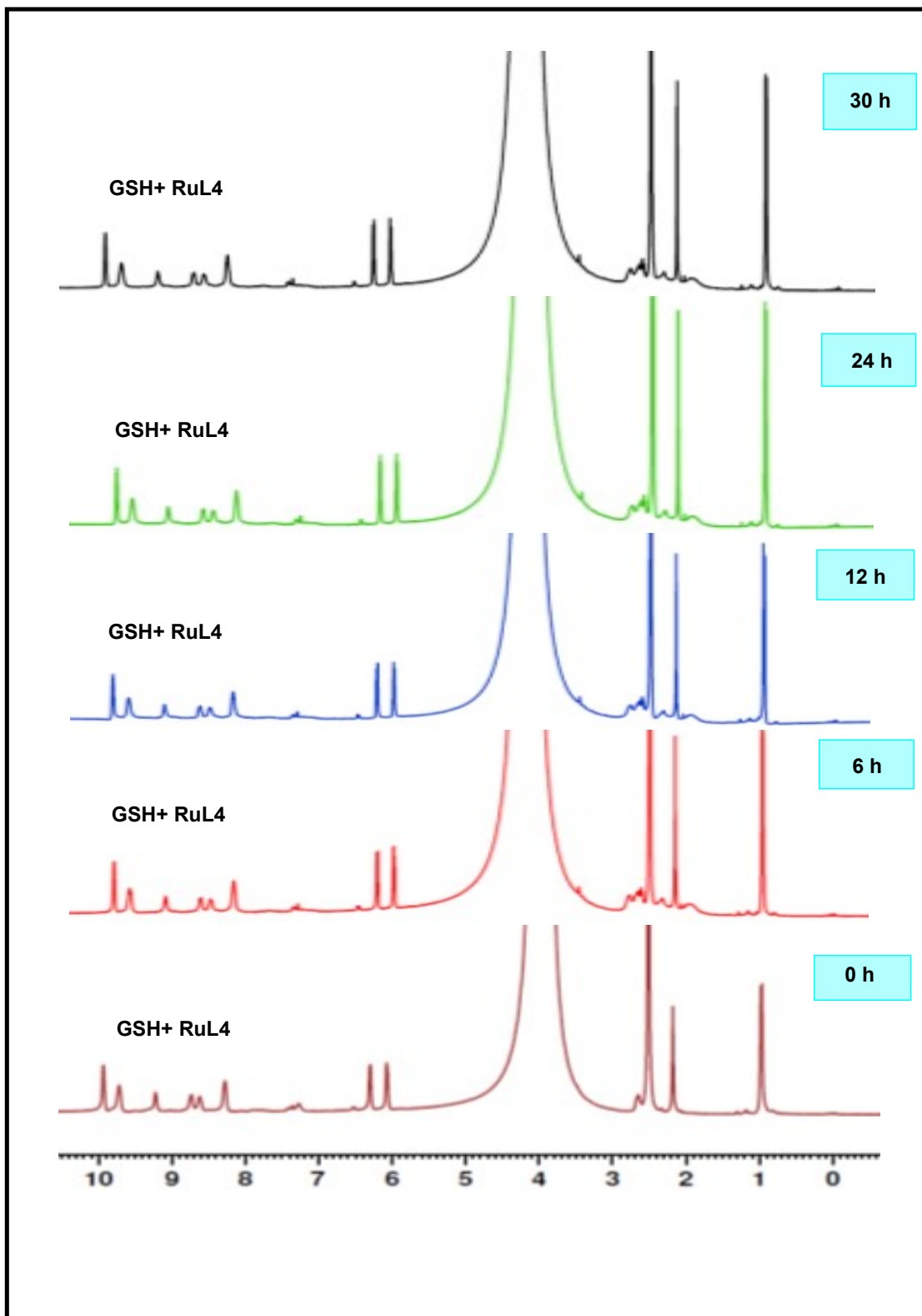
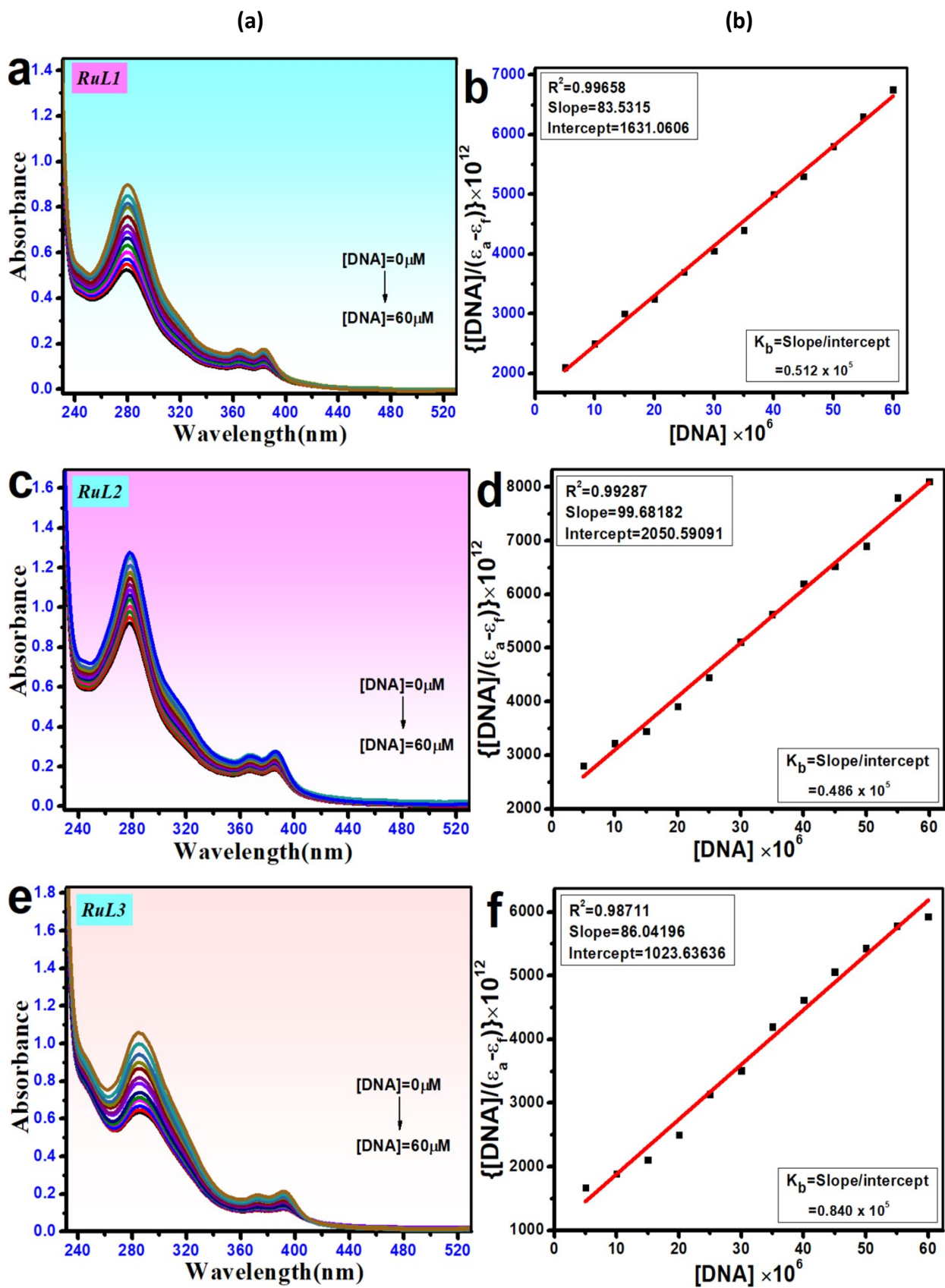


Fig. 11 Stability study of complex **RuL4** in presence of reduced L-glutathione and water *via* ¹H NMR. t = 0 h, stands for the spectra recorded immediately after dissolving reduced L-glutathione and complex.



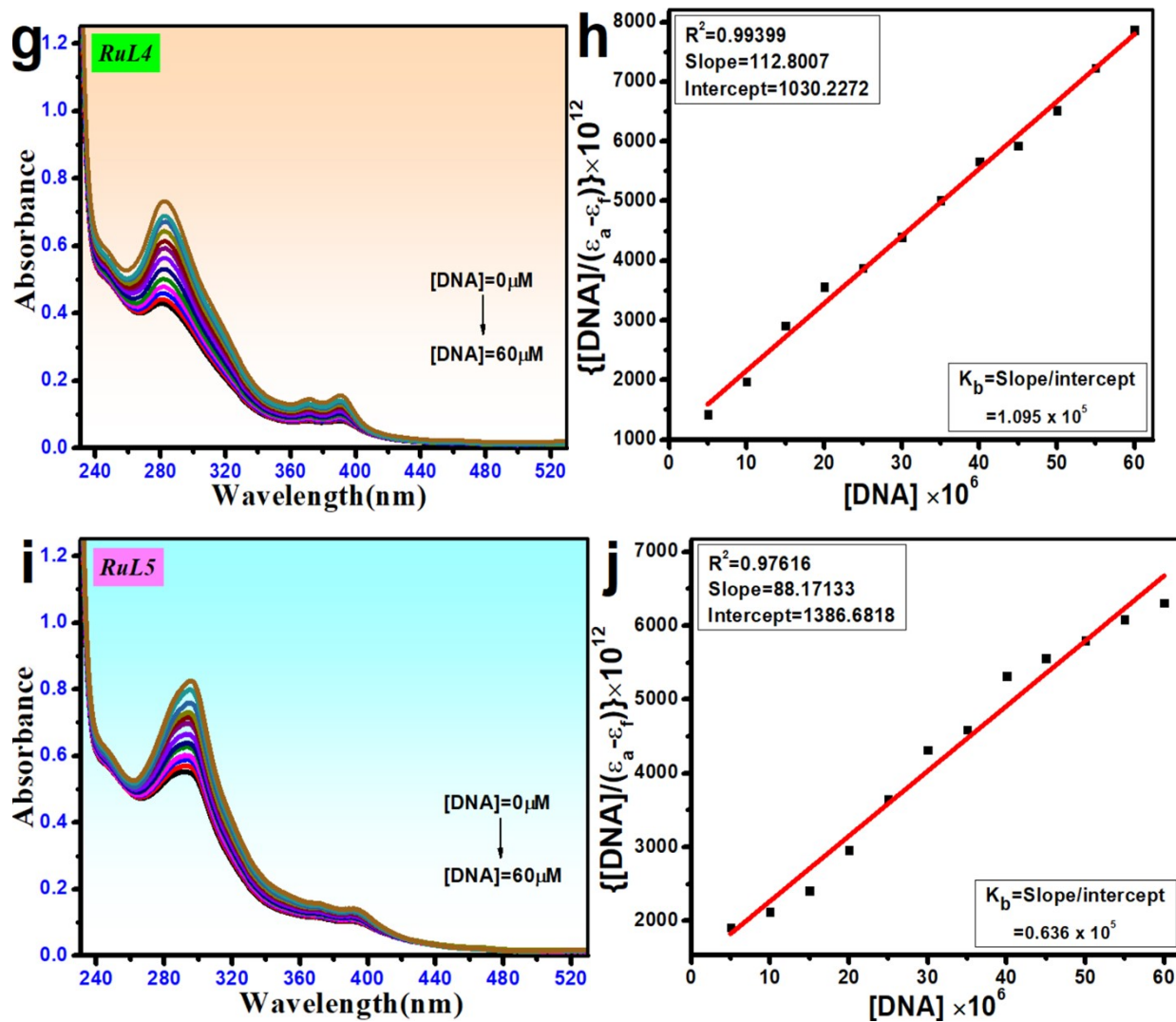
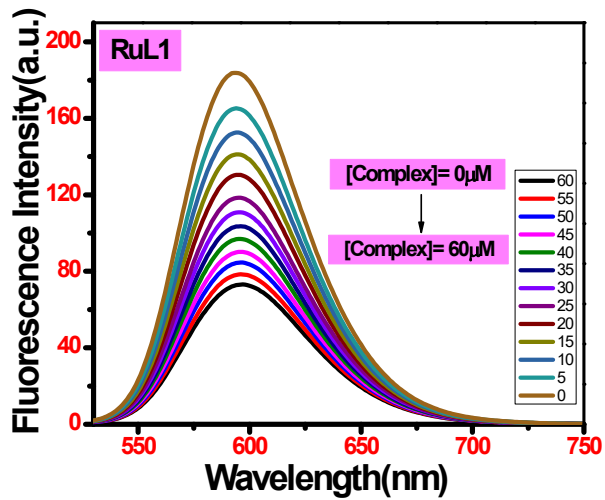
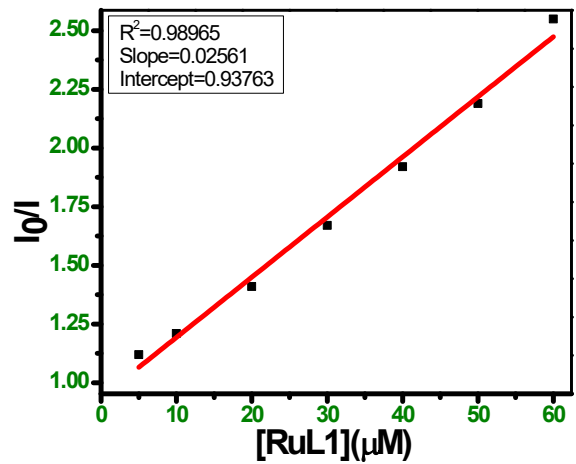


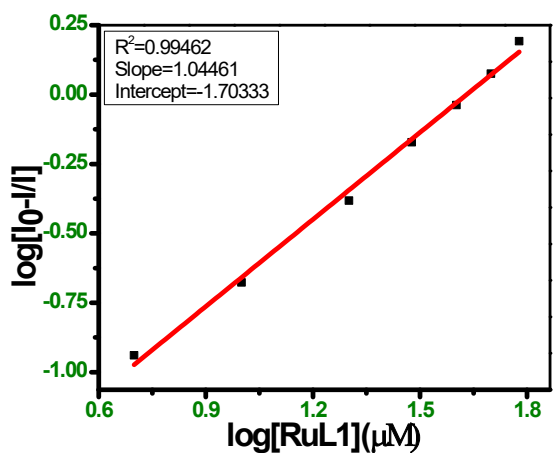
Fig. S12: DNA binding plots of all five complexes [(a), (c), (e), (g), and (i)]. $[DNA]/(\epsilon_a - \epsilon_f)$ vs. $[DNA]$ linear plots of all five complexes [(b), (d), (f), (h), and (j)].



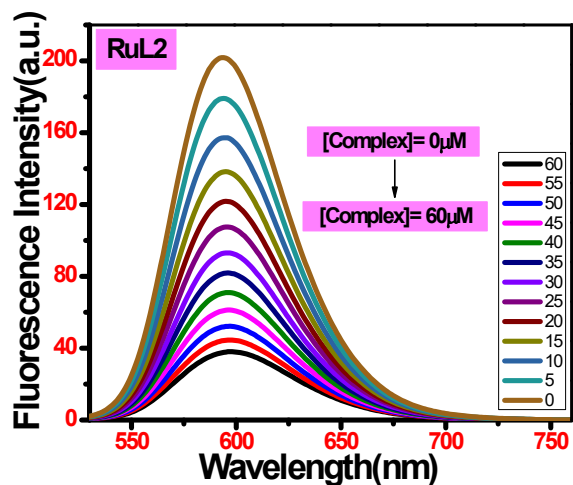
(a)



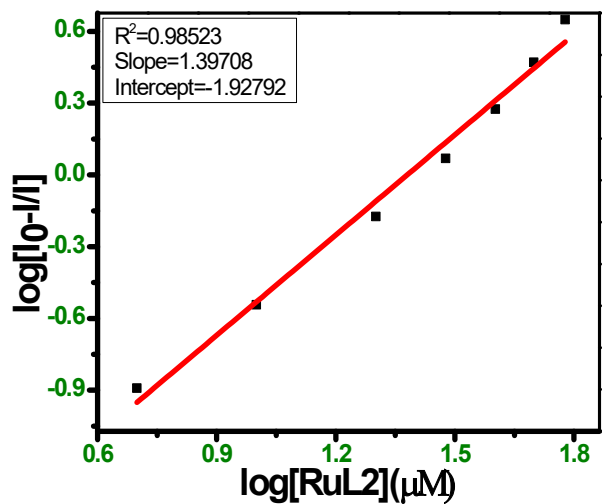
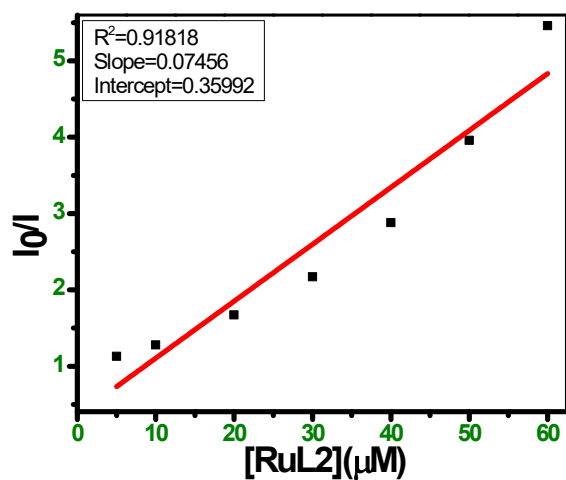
(b)

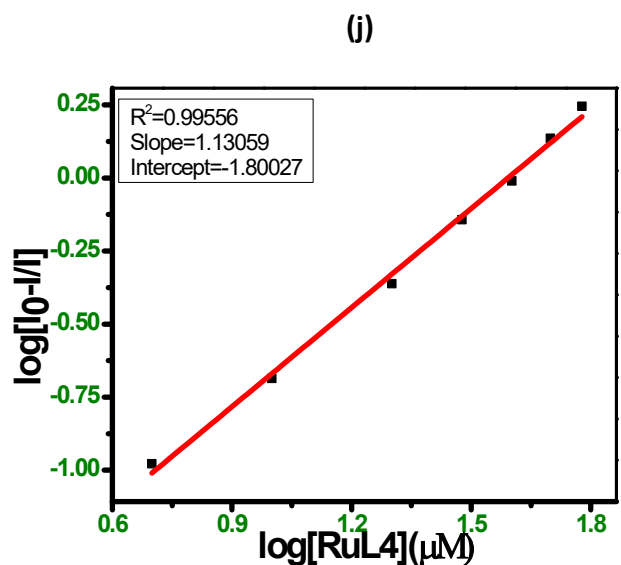
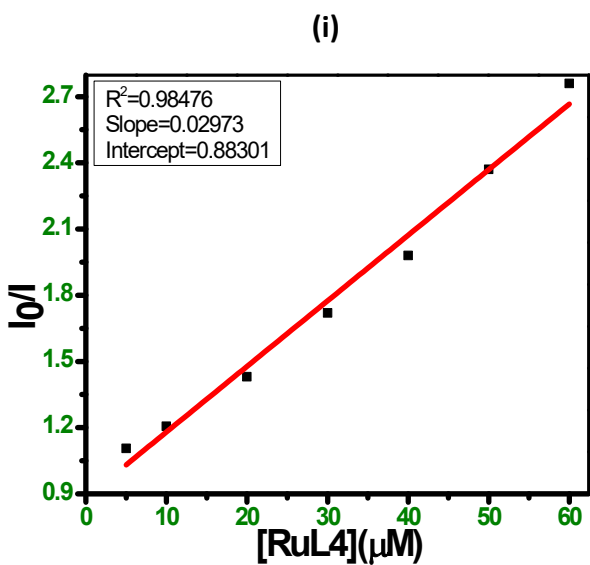
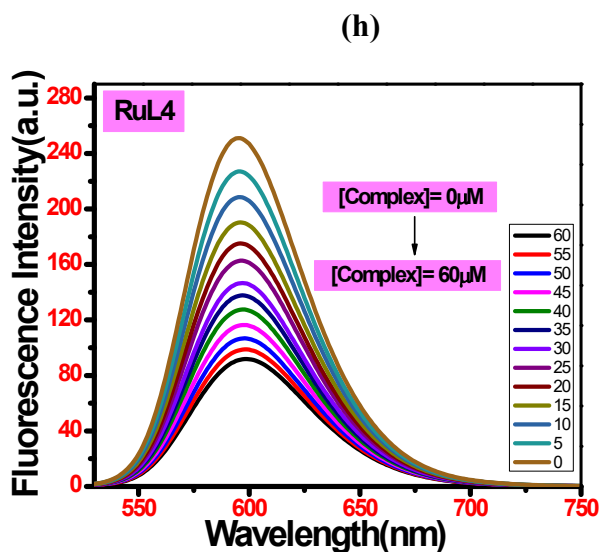
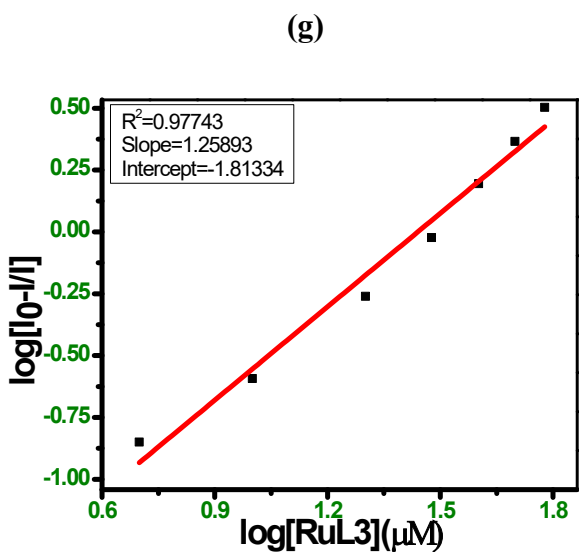
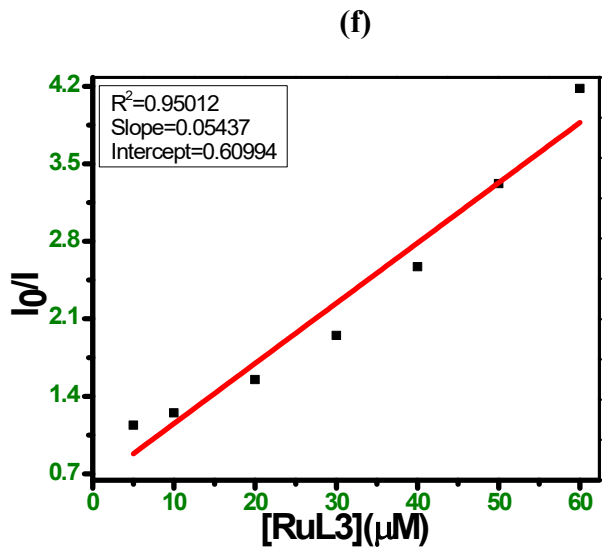
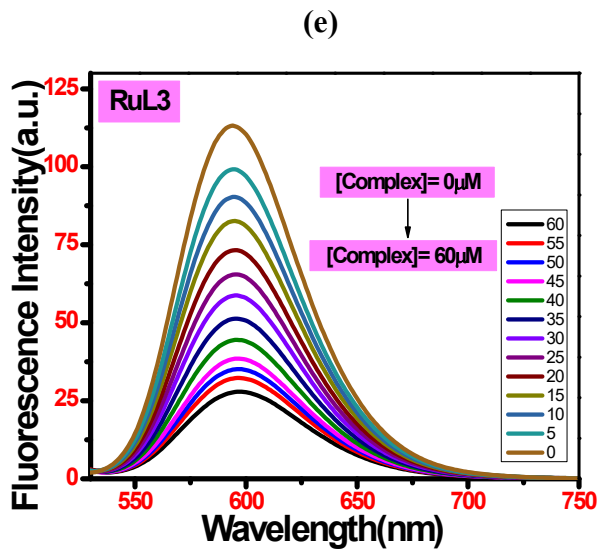


(c)



(d)





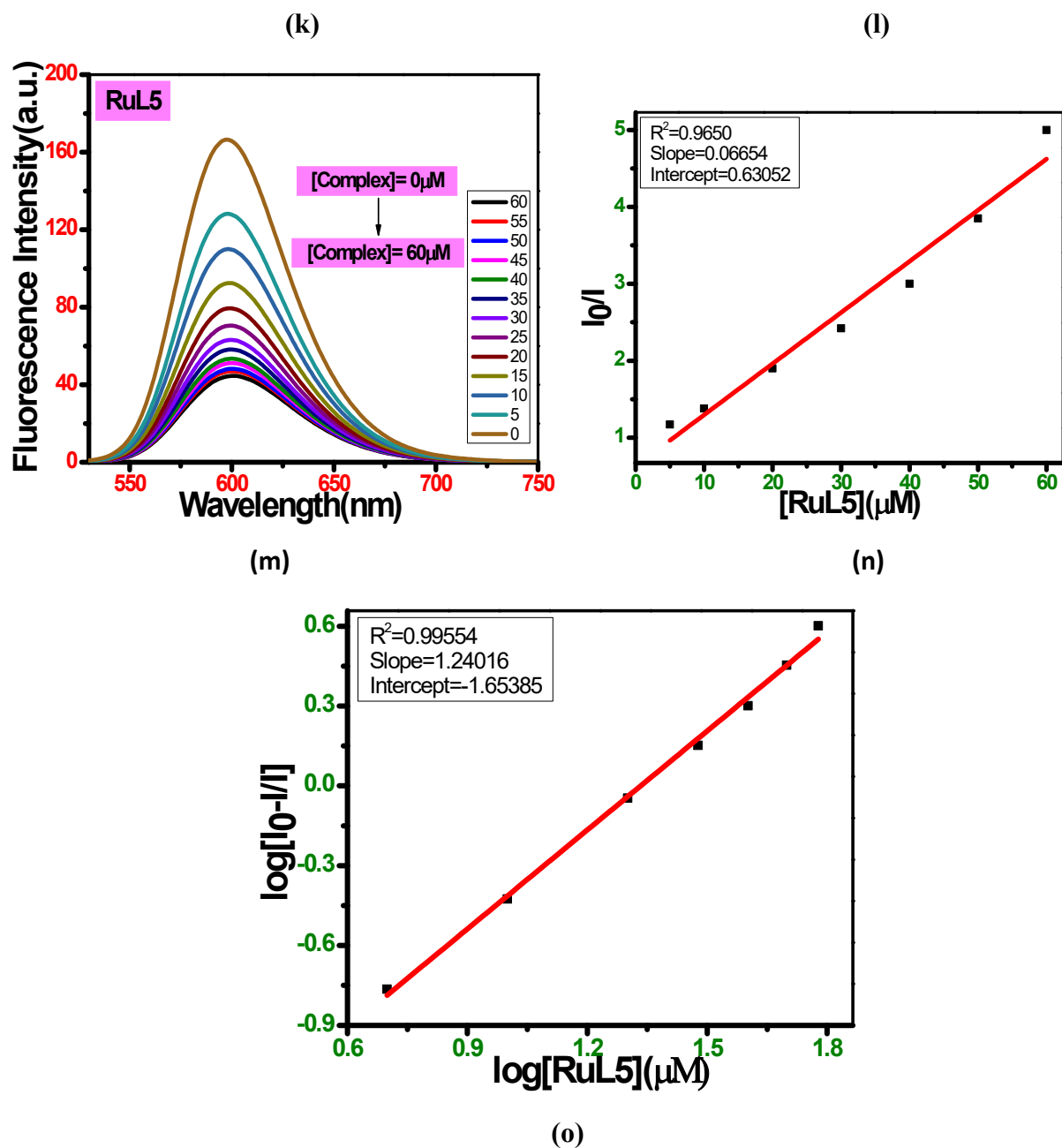
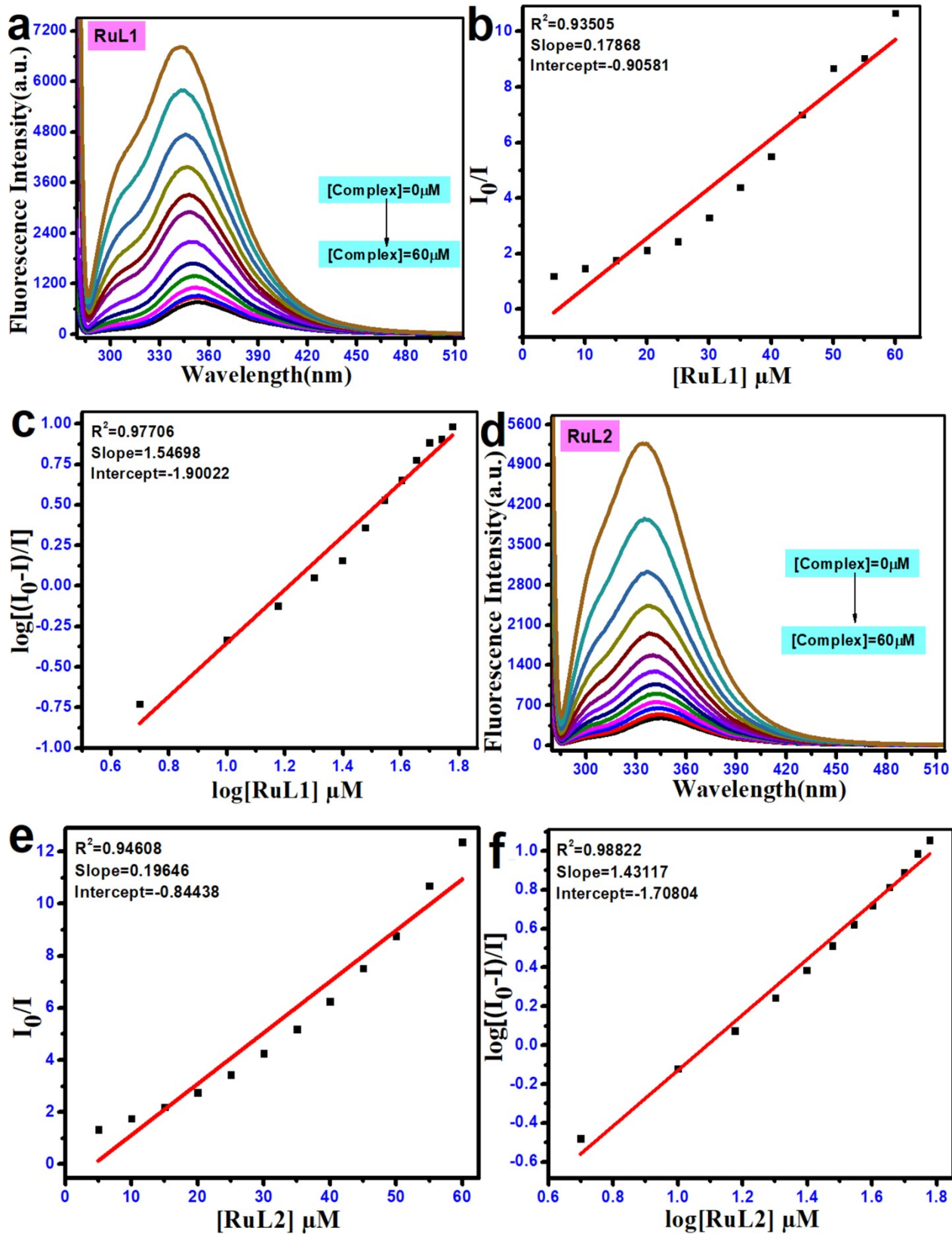
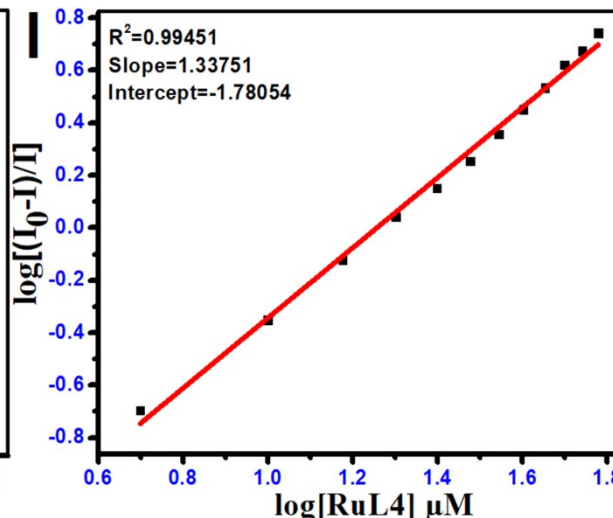
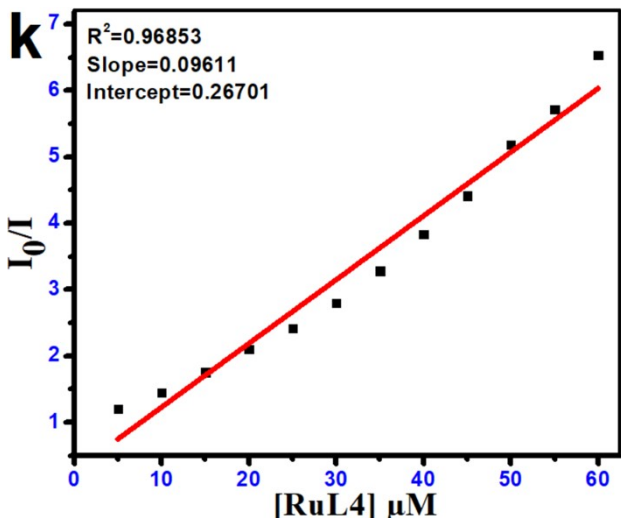
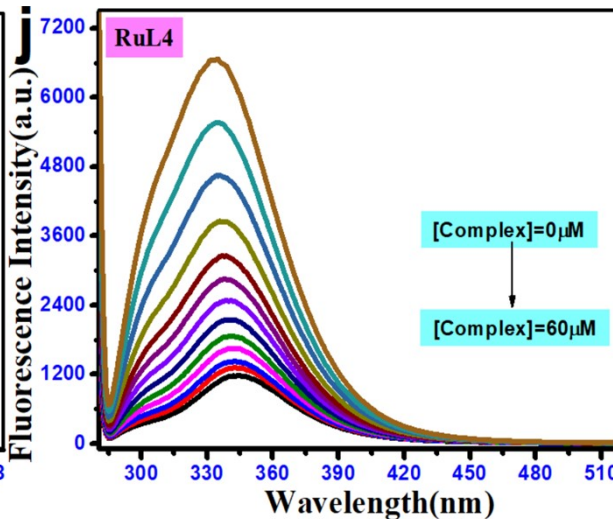
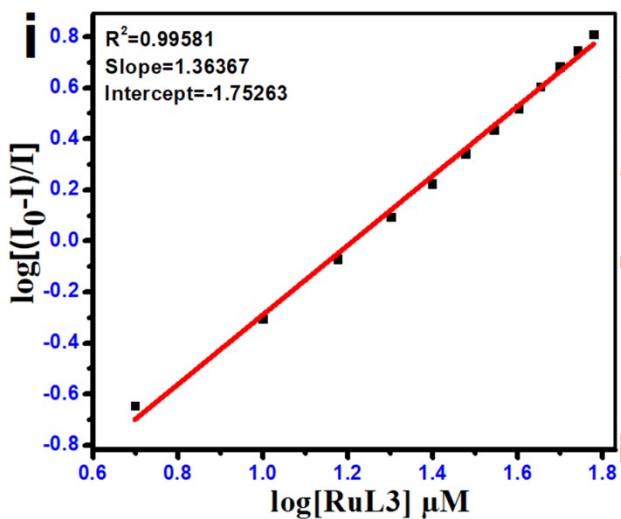
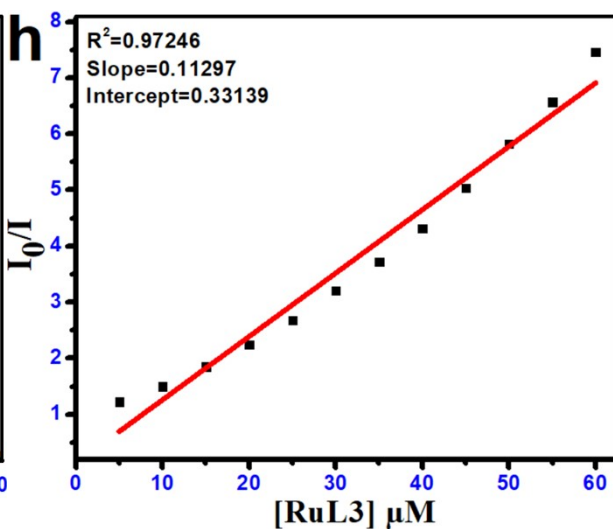
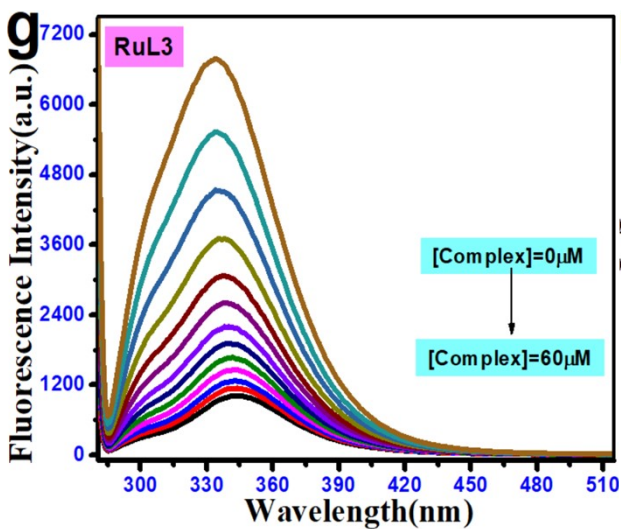


Fig. S13: Interaction of all five complexes with EtBr [(a), (d), (g), (j), and (m)]. Stern-Volmer Plot of I_0/I vs. concentration of complex [(b), (e), (h), (k), and (n)]. Scatchard Plot of $\log([I_0-I]/I)$ vs. $\log[\text{Complex}]$ for EtBr in the presence of metal complexes [(c), (f), (i), (l), and (o)].





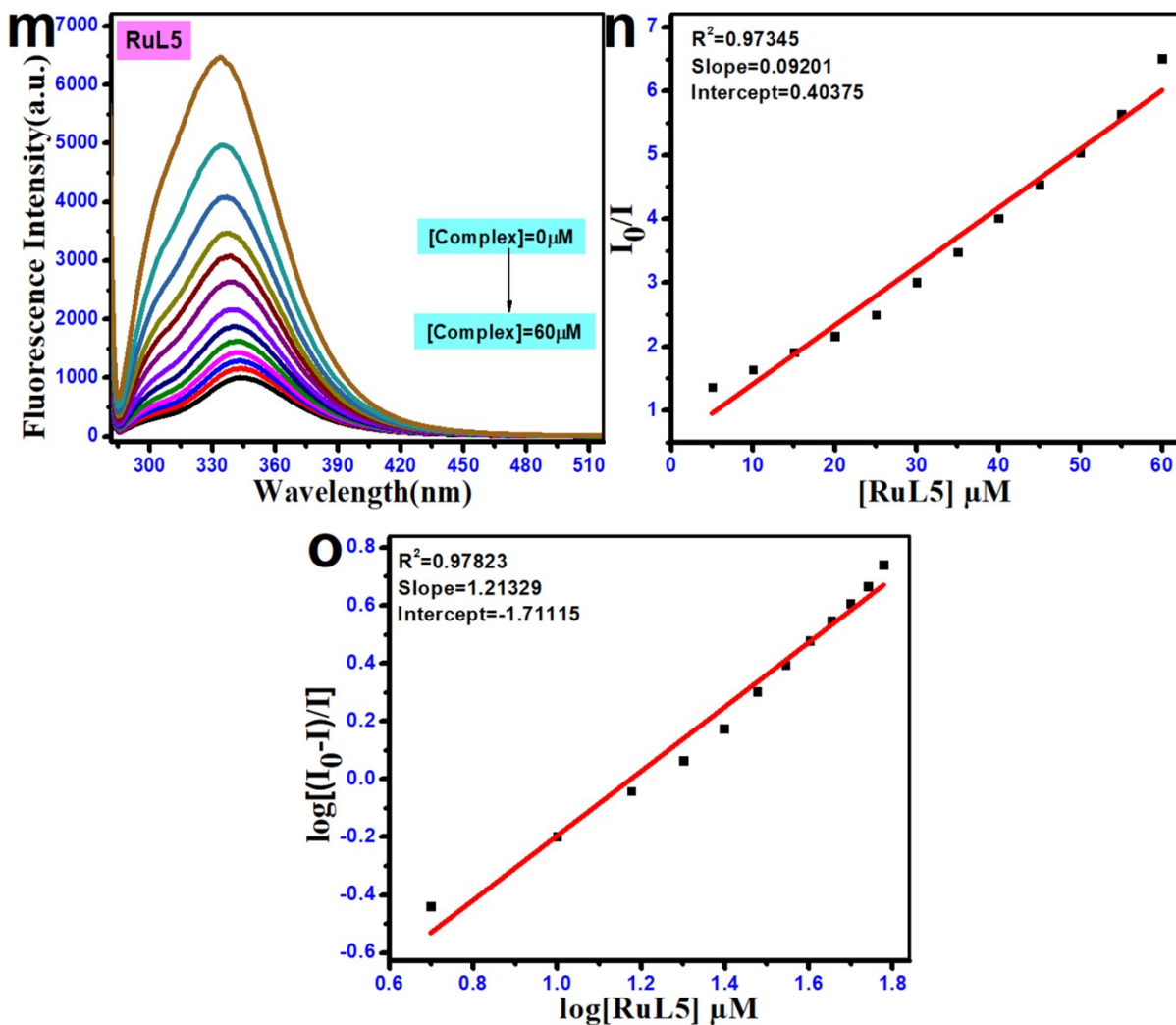


Fig. S14: Interaction of all five complexes with HSA [(a), (d), (g), (j), and (m)]. Stern-Volmer Plot of I_0/I vs. concentration of complex [(b), (e), (h), (k), and (n)]. Scatchard Plot of $\log[(I_0-I)/I]$ vs. $\log[\text{Complex}]$ for HSA in the presence of metal complexes [(c), (f), (i), (l), and (o)].

Experimental Section

DNA binding study

Electronic absorption spectroscopy was employed to study the binding capacity of the complexes with calf-thymus DNA (Ct-DNA) and competitive binding assay as studied using ethidium bromide (EtBr) as quencher by fluorescence spectroscopy.

UV-visible studies¹

DNA binding assay was carried out by using complexes **[RuL1-RuL5]** in Tris-HCl buffer (5 mM Tris-HCl in water, pH 7.4) in aqueous medium. The concentration of CT-DNA was calculated from its absorbance intensity at 260 nm and its known molar absorption coefficient value of 6600 M⁻¹ cm⁻¹. Equal amount of DNA was added in both the sample and reference in cuvettes. Titration was carried out by increasing concentration of CT-DNA. On the eve of each measurement, sample was equilibrated with CT-DNA for about 5 min and then absorbance of the complex was measured. The intrinsic DNA binding constant (K_b) was calculated using the equation (i):

$$\frac{[DNA]}{(\varepsilon_a - \varepsilon_f)} = \frac{[DNA]}{(\varepsilon_b - \varepsilon_f)} + \frac{1}{K_b(\varepsilon_a - \varepsilon_f)}L \quad (i)$$

Where [DNA] is the concentration of DNA in the base pairs, ε_a is the apparent extinction coefficient observed for the complex, ε_f corresponds to the extinction coefficient of the complex in its free form, and ε_b refers to the extinction coefficient of the complex when fully bound to DNA. The resultant data were plotted using Origin Lab, version 8.5 to obtain the [DNA]/($\varepsilon_a - \varepsilon_f$) vs. [DNA] linear plot. The ratio of the slope to intercept from the linear fit gave the values of the intrinsic binding constants (K_b).

Photophysical study

UV and Fluorescence study of all these Ru(II) complexes were executed in 10 % DMSO solution. Then the fluorescence quantum yields (Φ) were calculated by applying the comparative William's method which involves the use of well-characterized standard with known quantum

yield value using 10% DMSO solution.² Quinine sulphate was used as a standard. Quantum yield was calculated according to the equation (ii):

$$\varphi = \varphi_R \times \frac{I_S}{I_R} \times \frac{OD_R}{OD_S} \times \frac{\eta_S}{\eta_R} \dots\dots(ii)$$

Where, φ = quantum yield, I = peak area, OD = absorbance at λ_{max} , η = refractive index of solvent (s) and reference (R). Here, we have used quinine sulphate as a standard for calculating the quantum yield.

Ethidium bromide displacement assay

The ethidium bromide (EtBr) displacement assay was conducted to illustrate the mode of binding between the potent compounds with DNA.³ The apparent binding constant (K_{app}) of all the Ru(II) complexes to CT-DNA were calculated using ethidium bromide (EtBr) as a spectral probe in 5 mM Tris-HCl buffer (pH 7.4). EtBr do not show any fluorescence in its free state as its fluorescence is quenched by the solvent molecules. Nevertheless, its fluorescence intensity was radially increases with increase the concentration of CT-DNA, which suggested the intercalative mode of binding of EtBr with DNA grooves. The fluorescence intensity was found to decrease with further increase in concentration of the complexes. According to the displacement theory, it can be said that the complexes displaced EtBr from CT-DNA grooves and then bound to the DNA base pairs. The values of the apparent binding constant (K_{app}) were obtained by using the equation (iii):

$$K_{app} \times [Complex]_{50} = k_{EtBr} \times [EtBr] \dots\dots(iii)$$

Where K_{EtBr} is the EtBr binding constant ($K_{EtBr} = 1.0 \times 10^7 \text{ M}^{-1}$), and $[EtBr] = 8 \times 10^{-6} \text{ M}$. Stern-Volmer equation was followed for quantitative determination of the Stern-Volmer quenching constant (K_{SV}).⁴ Origin (8.5) software was used to plot the fluorescence data to obtain linear plot of I_0/I vs. $[complex]$. The value of K_{SV} was calculated from the following equation.

$$I_0/I = 1 + K_{SV} [Q] \quad (iv)$$

Where I_0 = fluorescence intensity in absence of complex and I = fluorescence intensities in presence of complex of concentration $[Q]$.

Protein binding studies

We are acquainted with the fact that serum albumin proteins are the main component. It is well known in blood plasma proteins and plays important roles in drug transport and metabolism, interaction of the drug with human serum albumin (HSA) was studied from tryptophan emission quenching experiment.⁵ Initially, HSA solution (2×10^{-6} M) was prepared in Tris-HCl/NaCl buffer. The aqueous solutions of the complexes were subsequently added to HSA solution with gradual increase of their concentrations. After each addition, the solutions were shaken slowly for 5 min before recording the fluorescence at a wavelength of 280 nm ($\lambda_{\text{ex}} = 280$ nm). A gradual decrease in fluorescence intensity of HSA at $\lambda = 345$ nm was observed upon increasing the concentration of complex, which confirmed that the interaction between the complex and HSA was happened. Stern-Volmer equation was employed to quantitatively determine the quenching constant (K_{HSA}). Origin Lab, version 8.5 was used to plot the emission spectral data to obtain linear plot of I_0/I vs. [complex] using the equation (v) given below:

$$I_0/I = 1 + K_{\text{HSA}} [Q] = 1 + k_q \tau_0 [Q] \dots \dots (v)$$

Where I_0 is the fluorescence intensity of HSA in absence of complex and I indicates the fluorescence intensity of HSA in presence of complex of concentration $[Q]$, τ_0 = lifetime of the tryptophan in HSA found as 1×10^{-8} and k_q is the quenching constant. Scatchard equation (vi) gives the binding properties of the complexes.⁶ Where K = binding constant and n = number of binding sites.

$$\log(I_0 - I/I) = \log K + n \log [Q] \dots \dots (vi)$$

Conductivity measurement⁷

For authenticating the interaction of the complexes with DMSO and aqueous DMSO, conductivity of the prepared complexes were performed using conductivity-TDS meter-307 (Systronics, India) and cell constant 1.0 cm^{-1} . Rate of conductivity was also estimated in different pH medium. Time dependent conductivity measurement was also carried out.

n-Octanol–water partition coefficient ($\log P_{o/w}$)⁸

The log $P_{o/w}$ of the Ru(II) complexes were adhering to shake flask method using the previously published procedure. A known amount of each Ru(II) complexes was suspended in water (pre-saturated with n-octanol) and shaken for 48 h on an orbital shaker. To allow the phase separation, the solution was centrifuged for 10 min at 3000 rpm. To obtain the partition coefficient, different ratios (0.5: 1, 1: 1, and 2: 1) of the saturated solutions were shaken with pre-saturated n-octanol for 20 min on an orbital shaker and followed the same procedure. Aliquots of the aqueous and octanol layers were pipetted out separately and the absorbances were measured with UV-Vis spectrophotometer using proper dilution. Each set was performed in triplicate, concentration of the substances in each layer was calculated using the respective molar extinction coefficients and the partition coefficient ($\log P_{o/w}$) values were obtained from the ratio.

Singlet oxygen (1O_2) quantum yield determination ⁹

The singlet oxygen (1O_2) quantum yields of the complex **RuL4** at ambient temperature in DMSO were determined using visible light (400–700 nm) for photosensitization. The 1O_2 quantum yields were determined by monitoring the photooxidation of DPBF after sensitization by the complex. DPBF is a convenient acceptor because it absorbs in the region where the dye is transparent and rapidly scavenges singlet oxygen to generate colorless products. This reaction occurs with little or no physical quenching. The solutions contained dyes in low concentrations and had optical densities ranging from 0.12 to 0.16 to minimize the possibility of 1O_2 quenching by the dyes. The photooxidation of DPBF was monitored from 20 s to 200 s. The 1O_2 quantum yield was calculated relative to optically matched solutions and comparing the quantum yield of DPBF photooxidation after sensitization by the compound of interest to that of Rose Bengal (RB) ($\phi[^1O_2]$ 0.76 in DMSO) as a reference compound according to Equation (vii).

$$\phi\Delta_c = \phi\Delta_{RB} \times m_c/m_{RB} \times F_{RB}/F_c \dots\dots\dots (vii)$$

where c denotes a complex, and RB denotes Rose Bengal. $\phi\Delta$ is the 1O_2 quantum yield, and m is the slope of the plot of DPBF absorbance at 417 nm vs. irradiation time. F is the absorption correction factor, which is given by Equation (viii).

$$F = 1 - 10^{-OD} \dots\dots\dots (viii)$$

Where, OD is the optical density at the irradiation wavelength.

Intracellular ROS Generation¹⁰

The intracellular ROS generation was studied by fluorescence assisted cell sorting using 2',7'-dichlorofluorescein diacetate (DCFDA) assay. In the typical assay, the HeLa cells are pre-treated with complex **RuL4** (10 μ M) for 4 h, followed by photoirradiation with red light (600–720 nm, 30 J/cm²) for an hour and then treated with DCFDA; finally, they are analyzed by EVOS M5000 fluorescent live cell imager (Thermo Fisher Scientific, USA).

Notes and References

1. M. Sirajuddin, S. Ali, A. Badshah, Drug–DNA interactions and their study by UV–Visible, fluorescence spectroscopies and cyclic voltammetry, *J. Photochem. Photobio. B.*, 2013, **124**, 1–19.
2. M. Shamsi-Sani, F. Hirini, SM. Abedini, M. Seddighi, Synthesis of benzimidazole and quinoxaline derivatives using reusable sulfonated rice husk ash (RHA-SO₃H) as a green and efficient solid acid catalyst, *Res. Chem. Intermed.*, 2016, **42**, 1091–1099.
3. S. Dasari, A. K. Patra, Luminescent europium and terbium complexes of dipyridoquinoxaline and dipyridophenazine ligands as photosensitizing antennae: structures and biological perspectives, *Dalton Trans.*, 2015, **44**, 19844–19855.
4. J. Keizer, Nonlinear fluorescence quenching and the origin of positive curvature in Stern-Volmer plots, *J. Am. Chem. Soc.*, 1983, **105**, 1494–1498.
5. V. D. Suryawanshi, L. S. Walekar, A. H. Gore, P. V. Anbhule, G. B. Kolekar, Spectroscopic analysis on the binding interaction of biologically active pyrimidine derivative with bovine serum albumin, *J. Pharm. Anal.*, 2016, **6**, 56–63.
6. K. Jeyalakshmi, J. Haribabu, C. Balachandran, S. Swaminathan, N. S. P. Bhuvanesh, R. Karvembu, Coordination Behavior of N,N',N''-Trisubstituted Guanidine Ligands in Their Ru–Arene Complexes: Synthetic, DNA/Protein Binding, and Cytotoxic Studies, *Organometallics*, 2019, **38**, 753–770.
7. S. Nikolić, L. Rangasamy, N. Gligorijević, S. Arandelović, S. Radulović, G. Gasser, S. Grgurić-Šipka, Synthesis, characterization and biological evaluation of novel Ru(II)–arene complexes containing intercalating ligands, *J. Inorg. Biochem.* 2016, **160**, 156–165.

8. M. Kubanik, H. Holtkamp, T. Söhnel, S. M. F. Jamieson, C. G. Hartinger, Impact of the Halogen Substitution Pattern on the Biological Activity of Organoruthenium 8-Hydroxyquinoline Anticancer Agents, *Organometallics*, 2015, **34**, 5658–5668.
9. M. Hoebeke, X. Damoiseau, 2002 Photochem. Photobiol. Sci., 2002, 1, 283.
10. (a) C. Evans, G. Malin, G. P. Mills, W. H. Wilson, VIRAL Infection of *Emiliana Huxleyi* (Prymnesiophyceae) Leads to elevated production of reactive oxygen species, *J. Phycol.*, 2006, **42**, 1040–1047. (b) S. Parveen, M. Hanif, E. Leung, K. K. H. Tong, A. Yang, J. Astin, G. H. De Zoysa, T. R. Steel, D. Goodman, S. Movassaghi, T. Söhnel, V. Sarojini, S. M. F. Jamieson, C. G. Hartinger, Anticancer organorhodium and -iridium complexes with low toxicity in vivo but high potency in vitro: DNA damage, reactive oxygen species formation, and haemolytic activity, *Chem. Commun.*, 2019, **55**, 12016.